

AD-A184 887

THE DESIGN AND ANALYSIS OF SINGLE FLANK TRANSMISSION
ERROR TESTER FOR LOA. (U) OHIO STATE UNIV COLUMBUS DEPT
OF MECHANICAL ENGINEERING D E BASSETT ET AL. JUN 87

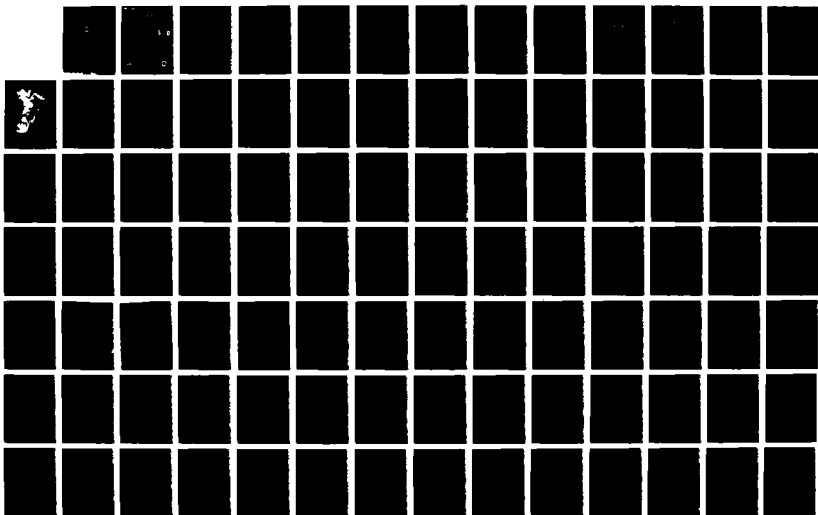
1/2

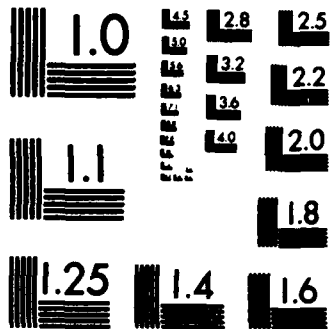
UNCLASSIFIED

NASA-CR-179621 NAG3-541

F/G 1379

NL





MICROCOPY RESOLUTION TEST CHART
NATIONAL BUREAU OF STANDARDS-1963-A

DTIC FILE COPY

NASA
Contractor Report 179621

AVSCOM
Technical Report 87-C-15

AD-A184 887

2

The Design and Analysis of Single Flank Transmission Error Tester for Loaded Gears

DTIC
ELECTE
SEP 17 1987
S **D**
C & D

Duane E. Bassett and Donald R. Houser
The Ohio State University
Columbus, Ohio

June 1987

DISTRIBUTION STATEMENT A

Approved for public release
Distribution Unlimited

Prepared for
Lewis Research Center
Under Grant NAG3-541

NASA
National Aeronautics and
Space Administration



87 9 16 089

TABLE OF CONTENTS

1. INTRODUCTION	1
1.1 Introduction	1
1.2 Previous Loaded Transmission Error Testers	2
1.3 Thesis Overview	11
2. GEAR ACCURACY	13
2.1 Introduction	13
2.2 Applications	14
2.3 Types of Geometrical Gear Errors	15
2.4 Gear Inspection	17
2.5 Transmission Error	21
2.6 Modification of Tooth Profile	26
2.7 Frequency Spectrum	26
3. LOADED TRANSMISSION ERROR SYSTEM DESIGN AND LAYOUT	28
3.1 Introduction	28
3.2 Optical Encoders and Signal Processing Unit	29
3.3 Test gear box	33
3.4 Drive Source and Load Motor	35
3.5 Feedback Transducers	41
3.6 Motor Controller and Amplifier	43
3.7 Couplings and Spacers	44
3.8 Base Plate	45
3.9 Installation of Equipment	46
4. DYNAMIC MODELING AND RESPONSE	49
4.1 Introduction	49
4.2 Dynamic Model and Equations	50
4.3 Open Loop Response	58
4.4 Proportional Control	67
4.5 Derivative Control	76
4.6 Integral Control	83
4.7 Closed Loop Response	83
4.8 Alternate Control Method	89
5. ALTERNATE TEST GEAR TYPES	91

5.1 Introduction	91
5.2 Bevel Gears	91
5.3 Worm Gears	94
5.4 Alternative Transmission Error Measurement Technique	94
6. Conclusions and Recommendations	96
6.1 Conclusions	96
6.2 Recommendations	97
Appendix A. DC TORQUE MOTORS	100
A.1 Introduction	100
A.2 Performance Characteristics	104
A.3 Operating Limits	106
Appendix B. TRANSMISSION ERROR MEASUREMENT	112
B.1 Introduction	112
B.2 Optical Encoders	112
B.3 Signal Processing of Transmission Error	117
Appendix C. COMPUTER PROGRAMS	126
Appendix D. COST ANALYSIS	130

Accession For	
NTIS CRA&I	<input checked="" type="checkbox"/>
DTIC TAB	<input type="checkbox"/>
Unannounced	<input type="checkbox"/>
Justification	
By	
Distribution/	
Availability Codes	
Dist	Avail and/or Special
A-1	

QUALITY INSPECTED
2

Chapter 1

INTRODUCTION

1.1 Introduction

Due to geometrical imperfections in gears and finite tooth stiffnesses, the motion transmitted from an input gear shaft to an output gear shaft will not have conjugate action. This non-uniform motion is termed transmission error and is an excitation of vibration and noise, two parameters which are of great interest to gear designers.

In order to strengthen the understanding of transmission error and to verify mathematical models of gear transmission error, a test stand that will measure the transmission error of a gear pair at operating loads, but at reduced speeds would be desirable. While most transmission error testers have been used to test gear pairs under unloaded conditions, it is the goal of this thesis to design a loaded transmission error tester.

A layout of the main components of such a test

stand is shown in Figure 1. For a gear box with a gear ratio of one, few tooth meshing combinations will occur during a single test. In order to observe the effects of different tooth mesh combinations and to increase the ability to load test gear pairs with higher gear ratios, the system was designed around a gear box with a gear ratio of two. It is desired that the motor and load be selected such that test conditions of up to 700 ft-lbf at 6 rpm on the drive side and 1,400 ft-lbf at 3 rpm on the load side (for a gear ratio of 2) are possible for a test time of at least one hour. This will enable the test stand to test a gear pair of 7.5 inch center distance, 12 diametral pitch, 2:1 gear ratio) with a face width of 2.5 inches at design loads as calculated by the AGMA Gear Strength Rating 218.01 [1].

1.2 Previous Loaded Transmission Error Testers

As previously noted, most transmission error testers have nominal torque capabilities, yet beginning with Harris [6] in 1958, some loaded testers have been reported. This section reviews, in increasing load capability, several of the loaded test stands that have been reported in the literature.

Hayashi and Hayashi [7] basically used the same

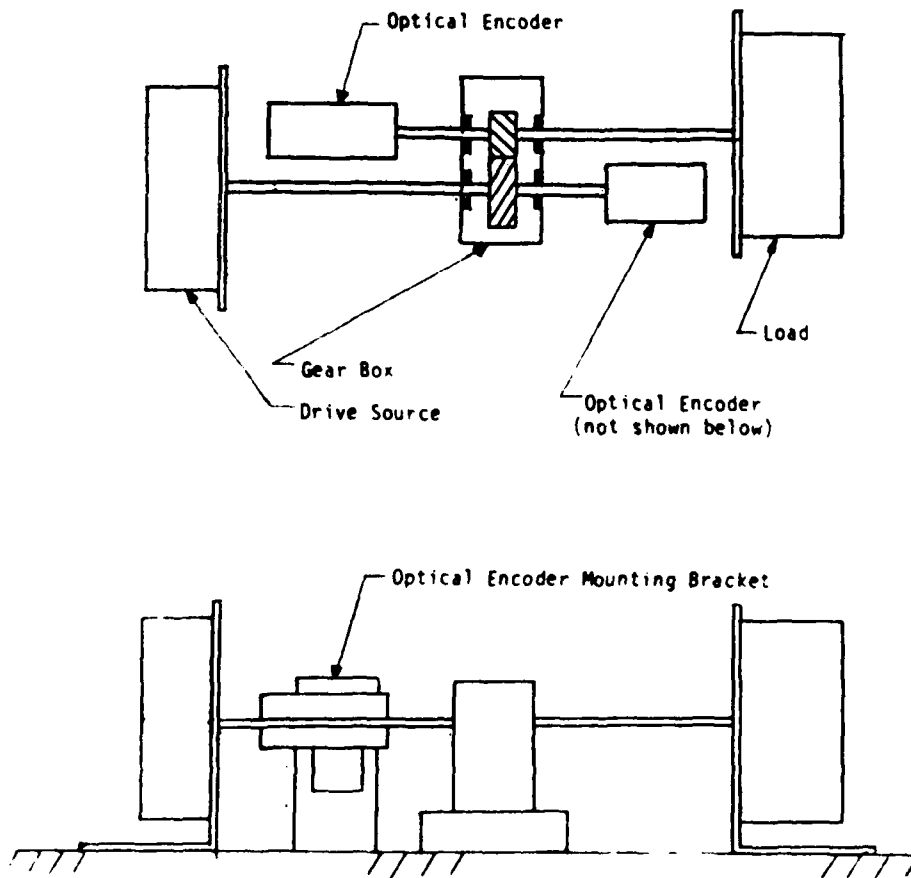


Figure 1: Test Stand Layout

layout as in Figure 1, but the torque transmitted was under 5 ft-lbf, while the maximum test speed was 1,500 rpm. They inserted a flywheel in between the gear box and the motor and the gear box and the load, and solved the system dynamic equations, assuming negligible gear inertias and system damping, for θ_2 and θ_3 (the angle of the pinion and the gear) with torque inputs T_1 , T_2 , T_3 , and T_4 as shown in Figure 2. The torques were measured with strain gages and fed into integrators and potentiometers to calculate each angle and by subtracting the two angles, the transmission error was calculated. They reported, "sufficient accuracy for practical use."

Daly [2] did extensive research using a recirculating power rig (four-square rig) which is shown in Figures 3 and 4. Daly used optical encoders to measure the transmission error. He tested two gear boxes: an automotive type manual transmission and a gear box with one pair of spur gears. Maximum torque loading was 90 ft-lbf, while a DC motor using a V-belt drive was used to produce test speeds from zero to 6,000 rpm. In both cases a flexible coupling needed to be inserted between the gear train being tested and one of the four-square gear boxes to reduce the effect of slave

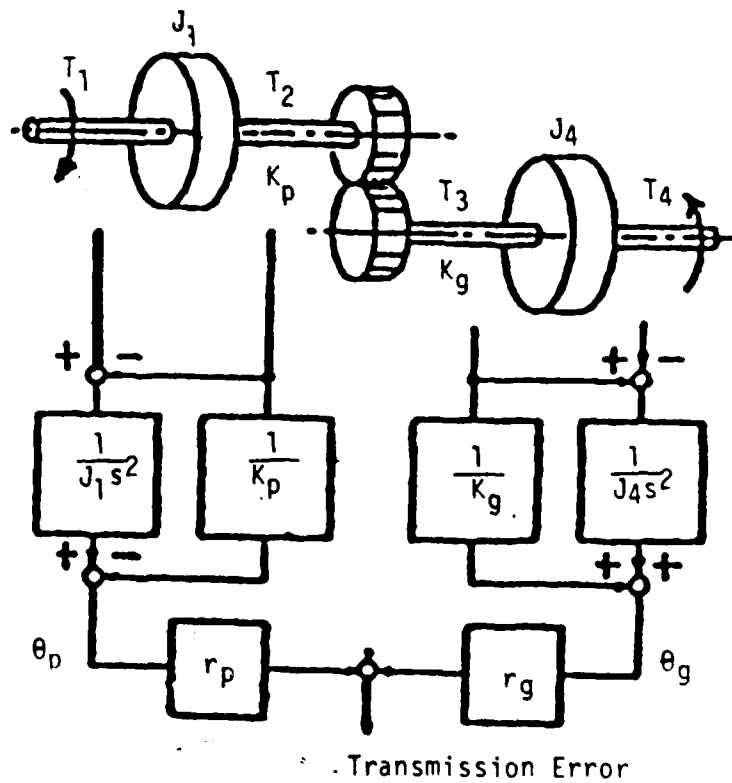


Figure 2: Hayashi and Hayashi's method of calculating transmission error; Hayashi [7]

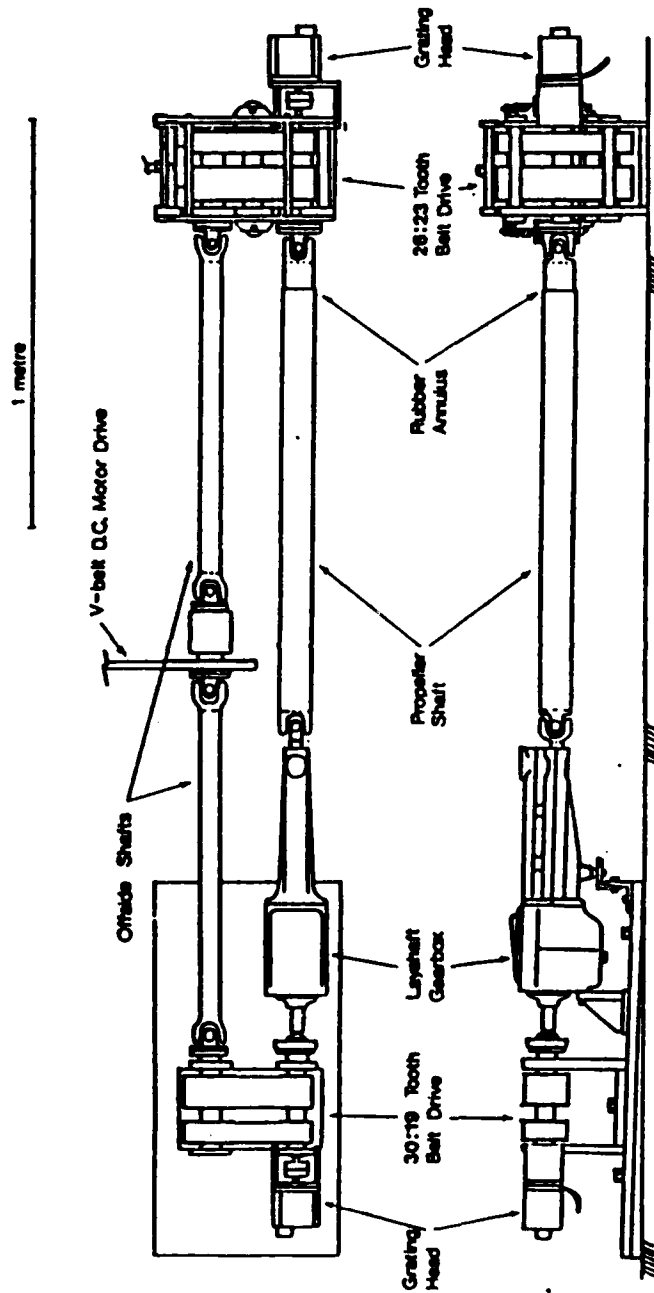


Figure 3: Layout of Dally's Four-Square Test Stand for a Manual Transmission after Dally [2]

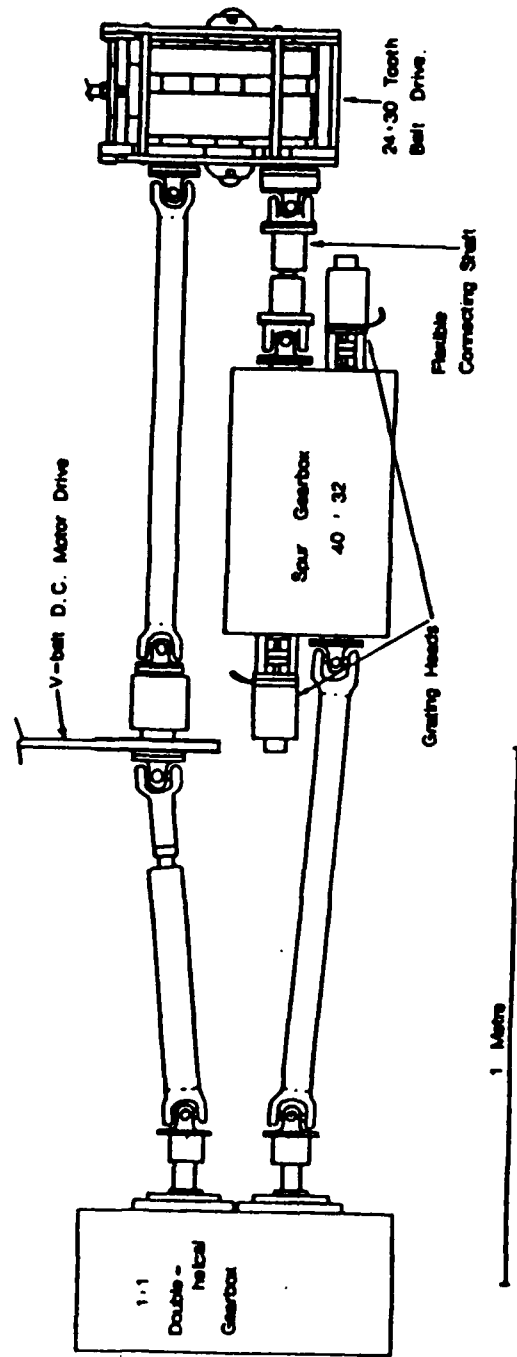


Figure 4: Layout of Daly's Four-Square Test Stand for a Spur Gear Pair after Daly [2]

gear box vibrations on the transmission error measurements.

Seager [15] used a four-square test stand and optical encoders shown in Figure 5 to measure the transmission error of a gear pair. He showed that the torsional vibration amplitudes of a spur gear pair are about four times the magnitude of a comparable helical gear pair for loads up to 500 ft-lbf. Seager confirmed the well-known fact, quantitatively, that helical gears can reduce vibrations compared to spur gears and should be used in high-duty applications.

Ichimaru and Hirano [9] also used a setup similar to Seager [15] to measure transmission error, but the thrust of their work involved tooth deformation and dynamic loading.

Lastly, Krenzer [12] constructed a test stand in which transmission error of an automotive rear axle loaded to torques up to 500 ft-lbf was measured at a mesh frequency of 12 Hz (Figure 6). Input torque to the rear axle was accomplished by driving an eddy current clutch with a 100 Hp, 3,500 rpm AC motor, while the load was supplied by an eddy current brake. Krenzer assumed the input speed of the gear pair to be constant and measured only the acceleration of the output shaft. The

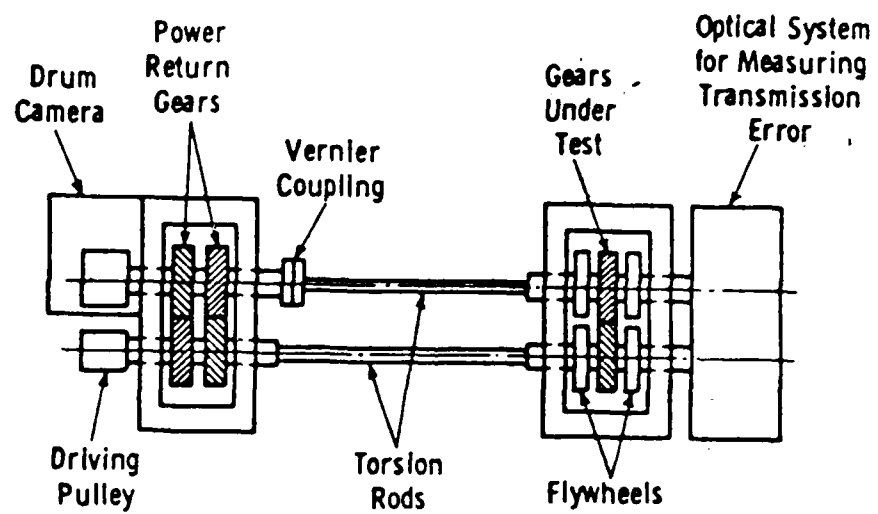


Figure 5: Seager's Four Square Test Stand; after Seager [15]

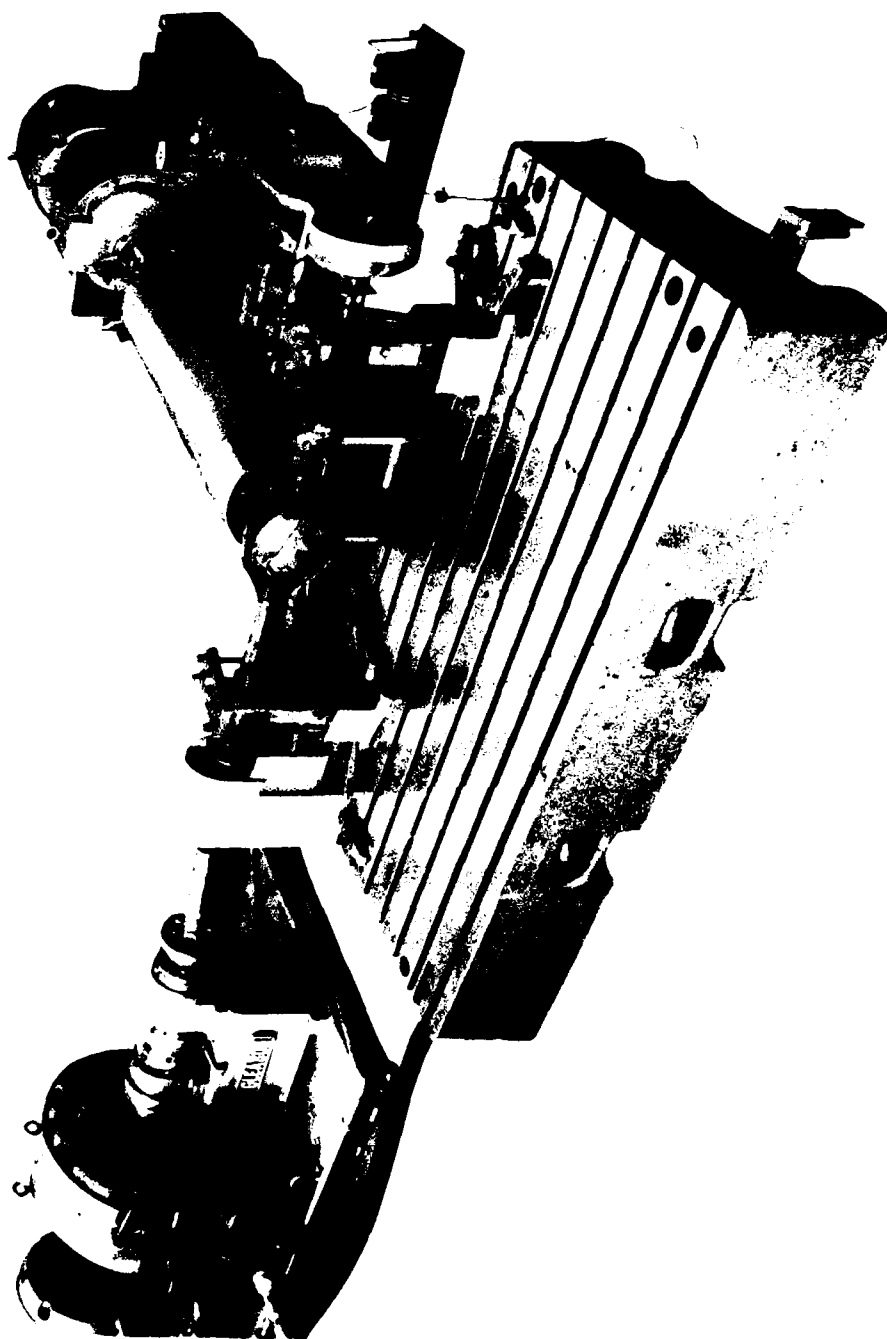


Figure 6: Krenzer's Rear Axle Transmission Error Tester; after Krenzer [12]

acceleration was integrated twice to determine the output angular position and transmission error.

1.3 Thesis Overview

The purpose of this thesis was to design a system to measure the transmission error of a set of spur or helical gears under loaded conditions. The torque and speed specifications were mentioned briefly in Section 1.1 and will be elaborated on further in Chapter 4.

Chapter 2 gives background information on gear errors and gear error measurement techniques. Chapter 3 discusses the test stand design and layout. Dynamic analysis of the system, including torque and speed control methods and error analysis, is covered in Chapter 4. Chapter 5 discusses the possibility of testing bevel gears and worm gears with the tester. The final chapter, Chapter 6, contains recommendations and a summary of the test stand design features.

Five appendices are included. Appendix A is a synopsis of DC torque motors. Appendix B discusses optical encoders and the electronic calculation of transmission error from the output of the encoders. Appendix C contains the source listings of the computer programs used in Chapter 4, while Appendix D is a cost

analysis of the project.

Chapter 2

GEAR ACCURACY

2.1 Introduction

When the mating teeth in a gear train have profiles that produce a constant angular velocity ratio, they are said to be conjugate pairs. In theory, it is possible to select an arbitrary profile for a driving tooth, and then find a profile for the driven tooth which will give conjugate action. The involute profile is one solution which happens to have the same form for the driving and driven teeth. A benefit of the involute form is that conjugate action remains, even for small deviations in center distance, but since the involute profile is normally not perfect and other geometrical imperfections will exist, non-uniform motion is always present.

2.2 Applications

Geometrical imperfections in gears can significantly alter the ways in which motion and load are transmitted. A common requirement for servomechanisms, printing machinery, and some types of machine tools, is that angular motion should be transmitted with great precision [14].

For systems with higher loads and speeds, the non-uniform motion of gears creates an exciting force that will excite structural vibrations and cause noise [18]. Although the vibrations may lead to pitting and scoring of gear teeth, and reduced reliability of the gear train [13], the gear noise is often of primary interest. The noise generated will depend on the transmission error of the gear pair, shaft speeds and loads, and the mechanical properties of the gear box.

The noise produced from the gear box is generally proportional to the load, but for spur gears Harris [6] showed that an optimum load often exists which results in a reduced noise level. The optimum load gives rise to the smoothest motion, or lowest transmission error for the gear pair and will usually exist for gears with profile modifications. For loads less than the optimum load, especially for unloaded or

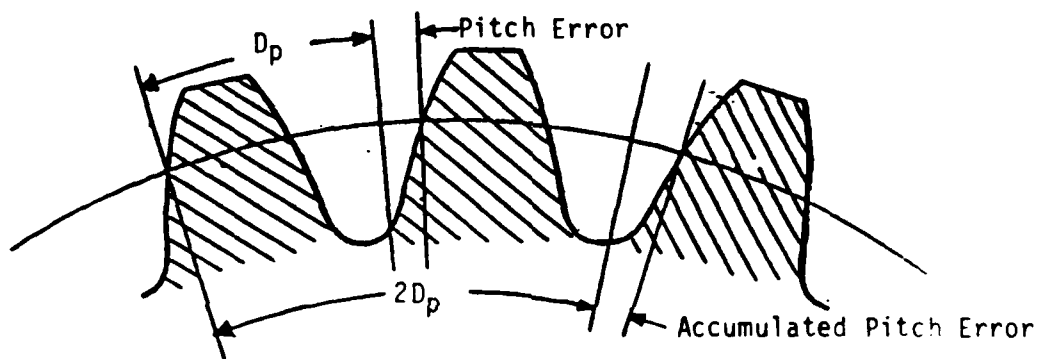
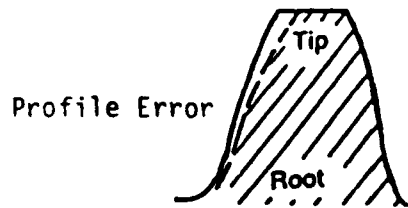
lightly loaded shafts, the teeth bounce about and may not remain in contact to produce noises which are made up of tooth impacts.

Noise reduction may be achieved by increasing the contact ratio such that additional pairs of teeth are always in contact (e.g. from 1.7 to 2.3). In troublesome cases with spur gears, vibration and noise can be reduced by changing to helical gears where the load transfer from tooth to tooth is smoother due to the increased load sharing. Therefore, stiffness variations and static transmission error variations are greatly reduced compared with spur gears, and consequently, helical gears are less prone to large vibrations [15].

2.3 Types of Geometrical Gear Errors

For spur and helical gears the geometrical errors that may exist are listed below. Items 1-4 are shown in Figure 7.

1. Involute (or profile) error - Tooth forms that differ from the ideal involute.
2. Pitch error - The angular position error of one tooth relative to an adjacent tooth. May also be expressed in distance at the pitch radius.
3. Accumulated pitch variation - The error in distance along the pitch circle radius that



D_p = Design Pitch

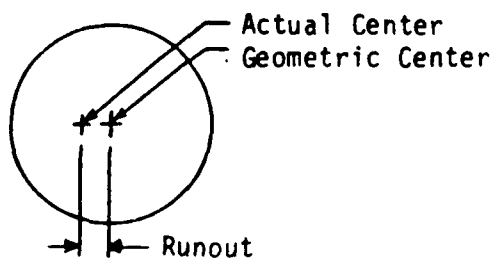


Figure 7: Geometrical Errors of Gear Teeth; after Smith [18]

the tooth is offset relative to an initial tooth.

4. Runout - The amount of eccentricity between the shaft center and the pitch circle due to imperfect mounting.
5. Lead error - The normal deviation from the design position of the tooth face in the axial direction.
6. Burrs on teeth.

Welbourn [20] has stated that better gears are likely to have a maximum runout of 0.0010 in., together with a maximum adjacent pitch error of 0.0002 in. and a maximum involute error of 0.0001 in. [20].

2.4 Gear Inspection

There are basically two types of gear inspection: elemental and composite. Elemental inspection involves the measurement of individual parameters of gear quality, usually by scanning the tooth face with a displacement measurement probe. Measured parameters typically include involute, lead or tooth alignment, pitch variation, runout, and tooth size. Newer gear inspection systems offer automated testing and on-line computer analysis for graphical output at resolutions as low as 1 micro-inch. Standard methods for measurement of individual errors have been widely used and are

adequate to define gear quality.

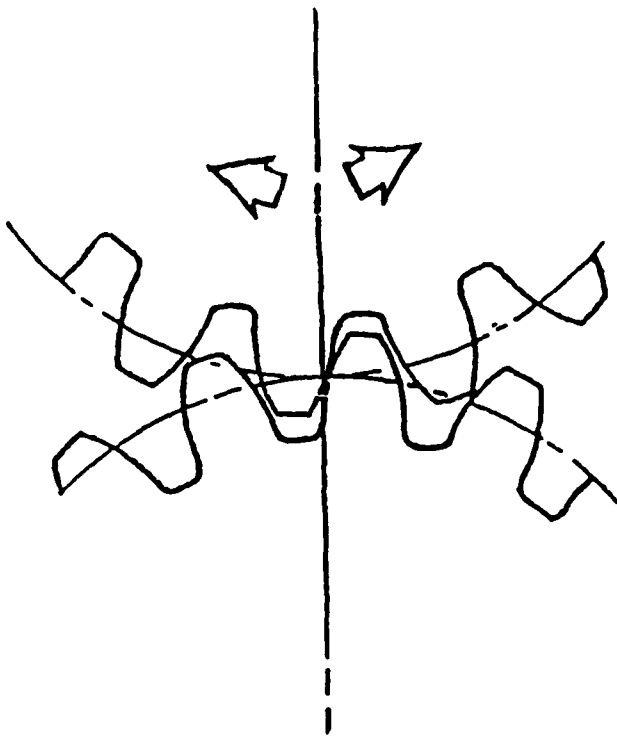
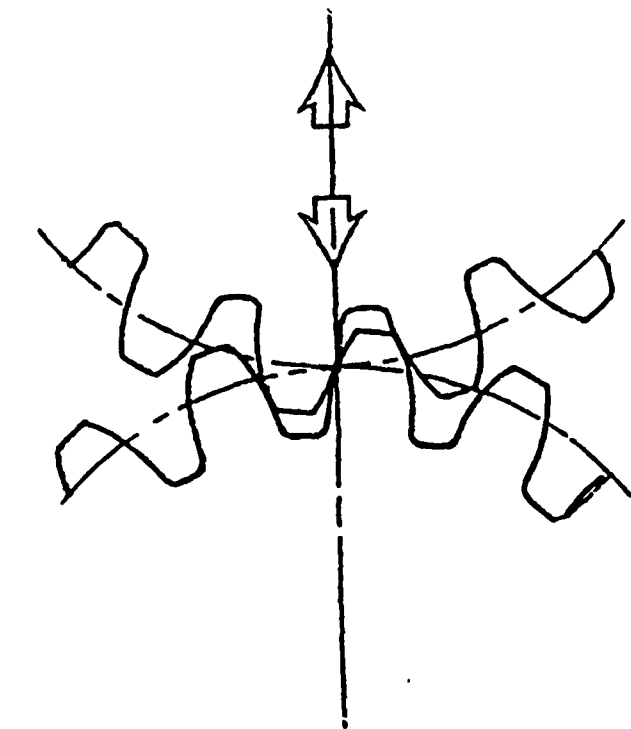
Composite testing involves meshing two gears together, one of which can be a master gear. Composite tests are attractive for inspection because they are quick and comprehensive in comparison with the conventional elemental methods in that most of the meshing surfaces are in nominal contact, rather than the discrete position measurement taken in elemental tests [14]. There are two types of composite tests: double flank and single flank (Figure 8).

The most common composite test is the double flank type in which two gears are meshed tightly on both sets of flanks so that there is no backlash. The variation in center distance is measured as the gears are rotated. As Munro [14] states, "This is a simple test, and for this reason, it is attractive, but it suffers from the difficulty that it is usually impossible to interpret the tooth-to-tooth pattern of the center distance variation curve in terms of elemental errors." Furthermore, the tight meshing conditions are not usually met in service and the double flank error curve is sometimes identical for two quite different sets of profile errors.

In single flank testing, the gears roll together,

Double Flank Gear Testing

Single Flank Gear Testing



Measures variation in center distance

Measures rotational movements

Figure 8: Double Flank and Single Flank Composite Test; after Smith [18]

as in service, at their proper center distance with only one flank of each gear in contact [18]. The recorded measurement is the difference in angular position, or transmission error. The measurement represents, as Daly and Smith [3] state, "the difference between the actual angular position of the output shaft of the gear pair and the position which the shaft would occupy if the gear pair were perfect, i.e. with no errors or deflections." Quantitatively, the transmission error is calculated as follows:

$$TE = \theta_p - n\theta_g \quad (2.1)$$

Where:

TE = transmission error

θ_p = angle of the driving gear (pinion)

θ_g = angle of the driven gear (gear)

n = gear ratio, N_g / N_p

N = number of teeth of the gear

The angle of each gear shaft may be measured in a variety of ways, but two of the more common methods use optical encoders (which is discussed in Appendix B) or angular accelerometers. The error may be given as an angular displacement in arc minutes or arc seconds, or as a linear displacement at the pitch circle radius in inches or millimeters.

2.5 Transmission Error

Transmission error does not have a single value, but should be thought of as a continuous variable, plotted as a curve versus gear rotation [14]. The transmission error can be considered to consist of the addition of two components: a mean value and an alternating value. Only the alternating component is of interest in gear noise. The mean component, which is due to the tooth deflection from the torque loading, will not give rise to a non-uniform motion, but will just cause a lag in angular position.

The measured transmission error is not of a single gear, but is measured for gear pair since the error contains contributions from each gear and is dependent upon the geometrical imperfections and tooth stiffness of each gear. However, one may select a drive gear whose geometrical imperfections are small compared to the driven or test gear. Such a gear is often referred to as a master gear. The transmission error of the gear pair will then approximate that of just the driven gear for unloaded or lightly loaded tests. For higher torque levels, and consequently larger deflections, a master gear is not likely to be as good an approximation of a perfect gear because its deflections differ little from

those of imperfect gears.

The processed transmission error data can be directly related to involute (profile) errors, pitch variation, runout, accumulated pitch variation, and burrs or loose debris. Only lead errors, which can affect the transmission error because they may cause the point of contact to travel axially across the tooth face, cannot be measured by this method.

If the gear pair under test does not contain a master gear, the once per tooth cycle errors on each gear cannot be identified from the transmission error measurement except when all gear tooth combinations occur. Then, according to Sharpe and Smith [16] time averaging techniques allow separation of the pitch errors. Otherwise, separate detailed gear measurement is necessary to locate these once per tooth mesh cycle errors which may be due to profile errors on either or both gears, due to helix angle errors, or due to alignment errors. A typical transmission error plot showing many of these errors is given in Figure 9.

The transmission error of a gear or gear pair is dependent on the direction of rotation, center distance, shaft speed, and the specific tooth pairs in contact. Since different flanks of the teeth are in contact, the

Individual errors revealed by single flank testing

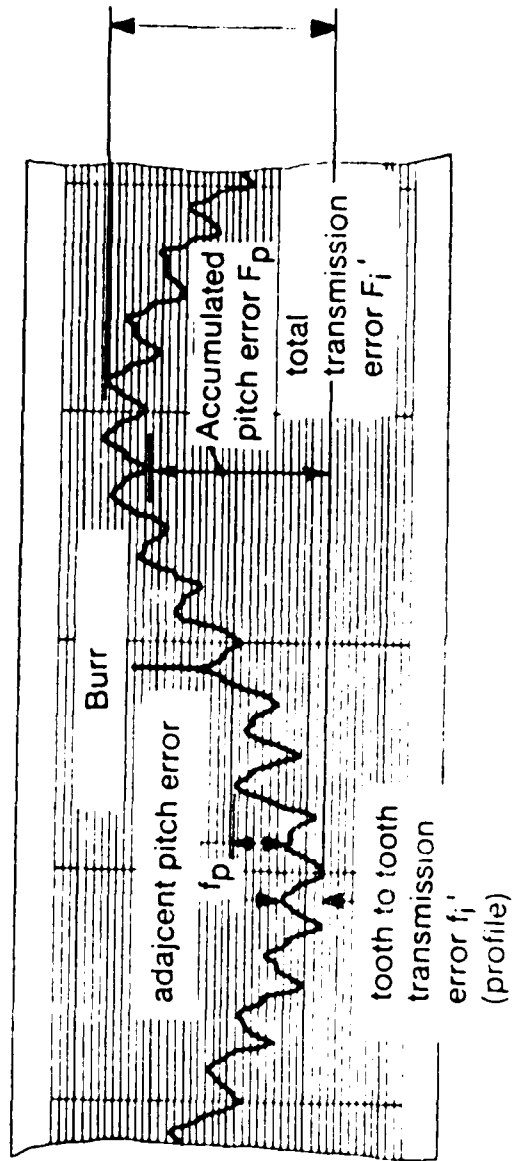


Figure 9: Typical Transmission Error Plot; after Smith [18]

transmission error is by no means identical for clockwise and counter-clockwise rotation. At the design center distance most of the gear face is in contact at one point or another, while for extended or contracted center distances different portions of the gear teeth will be in contact resulting in a different transmission error. The dependency of shaft speed is classified into two groups: static transmission error and dynamic transmission error. Static transmission error tests are run at very low shaft speeds (5-15 rpm), while dynamic transmission error tests are taken at normal operating speeds (typically 1000 rpm or higher). Constant shaft speed is not required since the error is a function of relative angular displacement and not of angular velocity, but the speed should not vary excessively in measuring transmission error. For a gear pair whose number of teeth on each gear do not have a least common denominator, each tooth on the driving gear will mesh with each and every tooth on the driven gear. Otherwise, only certain tooth mesh combinations will repetitively occur. The particular combinations may be changed by initially meshing with a different combination of gear teeth, hence, the transmission error will change.

Toda and Tordion [19] attempted to relate standard errors such as profile error, pitch error, etc. to transmission error using Fourier analysis. Their results showed that the combined pitch and profile error may be approximated as the transmission error, but as gear quality decreases, the difference between the gear transmission error and the combined pitch and profile errors becomes larger. Even for higher quality gears, differences between the single flank test and the combined pitch and profile errors will be present because it has been shown that there is some interaction between the elemental errors and because all of the tooth face does not mesh with its mating tooth [14].

In the past, the measurement of transmission error has been neglected, mainly due to the difficulty of conveniently measuring the small changes in relative shaft rotations which result from small imperfections [14]. Presently, the more complex transducers and their associated instrumentation required for single flank testing is relatively expensive, but has the advantage of being extremely accurate and requires little skill to use. Due to the high costs of the optical encoders, which are the usual sensing elements, the single flank test is not as common as the double

flank test, but since the single flank test is a much better indicator of gear noise and can distinguish elemental errors, Munro [14] believes it will ultimately be a measurement which is routinely made.

2.6 Modification of Tooth Profile

Sometimes it is beneficial to introduce small, intentional errors into the gear tooth profile. Because of the probable occurrence of unavoidable errors in the assembled gear train and because of tooth and housing deflections under load, high dynamic loads may result [18]. Therefore, it is usually necessary to modify the tooth shapes with tip, flank, and/or end relief which makes the tooth-to-tooth load transfer less abrupt. The benefits extend to transmission error as profile and lead modifications may also reduce the error, particularly the components at mesh frequency which are the main contributors to gear noise.

2.7 Frequency Spectrum

The transmission error curve is a periodic function, having distinct periodicities at once per each shaft revolution and once per tooth mesh cycle which can be conveniently represented by a Fourier series. The

errors at shaft speed frequency are typically due to pitch errors and eccentricities in mounting or manufacturing, while the mesh frequency (shaft speed multiplied by number of gear teeth) errors are due to profile errors and tooth stiffness changes which are similar from tooth to tooth. Multiples of the mesh frequency component are often present, while multiples of the shaft speed frequency are usually small compared to the fundamental frequency.

Gear noise reduction is normally achieved by reducing the frequency components at mesh frequency and its harmonics [8]. This is so because these frequencies are so often in the most sensitive frequency band of the ear [20] and are the largest in magnitude. When the speed of rotation is such that the frequency of one of the error components of the transmission error curve coincides with a natural frequency, high noise levels or large dynamic tooth loads, or both may result and should be avoided.

Chapter 3

LOADED TRANSMISSION ERROR SYSTEM DESIGN AND LAYOUT

3.1 Introduction

The goal in designing the loaded transmission error system was to be able to measure the transmission error of a gear pair under constant load and speed with minimal influences from the surroundings. It will be of interest to view the transmission error in both the time domain and the frequency domain. The time domain is useful in inspecting the transmission error on a tooth-to-tooth basis, while the frequency domain shows the components at mesh frequency and its harmonics which are particularly useful in gear noise analysis. This chapter discusses the selection of the specific hardware to be used and the physical layout of the equipment.

3.2 Optical Encoders and Signal Processing Unit

Restating equation (2.1) from chapter 2, transmission error is defined as follows:

$$TE = \theta_p - n\theta_g$$

Where:

θ_p = angle of driving gear (pinion)

θ_g = angle of driven gear (gear)

n = gear ratio, N_g / N_p

N = number of teeth on the gear

Therefore, the angular position of each gear must be measured (as continuous values), and then the transmission error may be calculated as given above (see appendix B for a detailed explanation).

The measurement of the angles will be made using high resolution, optical encoders which will be borrowed from an existing, unloaded (lightly loaded) transmission error tester made by Gleason/Goulder. The encoder heads have 18,000 lines per revolution which, after processing, enable the transmission error measurement to have a resolution of under 0.5 arc-seconds.

Integrated into one encoder is the drive source for the unloaded tester, a small DC torque motor, while a viscous damper which supplies a resisting torque, is

attached to the shaft of the other encoder. Since the torque motor will not be used, it will need to be disabled by disconnecting its four lead wires. The torque rating of the viscous damper is adjustable to a near zero setting and its effect on the transmitted torque will be negligible.

Each encoder head will be mounted on a 3 axis positioner as shown in Figure 10. The X and Y degrees of freedom are manifested by slots, while a screw drive controls the Z degree of freedom. Two T-slots, centered on the base plate and 45 inches apart, can be used to secure the mounting bracket to the base plate. Although there is sufficient area to mount the bracket to the base plate, the bracket will extend over the base plate.

The signal processing unit from the Gleason/Goulder unloaded tester will be used to calculate the transmission error from the output of the encoder heads. The processing unit has a frequency bandwidth from zero to 11 Hz and in most cases will provide the upper test speed limit. For analysis purposes the highest frequency to be recorded will, in general, be the third harmonic of mesh frequency. Hence, the maximum mesh frequency will be about 3.5 Hz, which, in turn, will limit the shaft speed, ω_1 , as stated in equation (3.1).

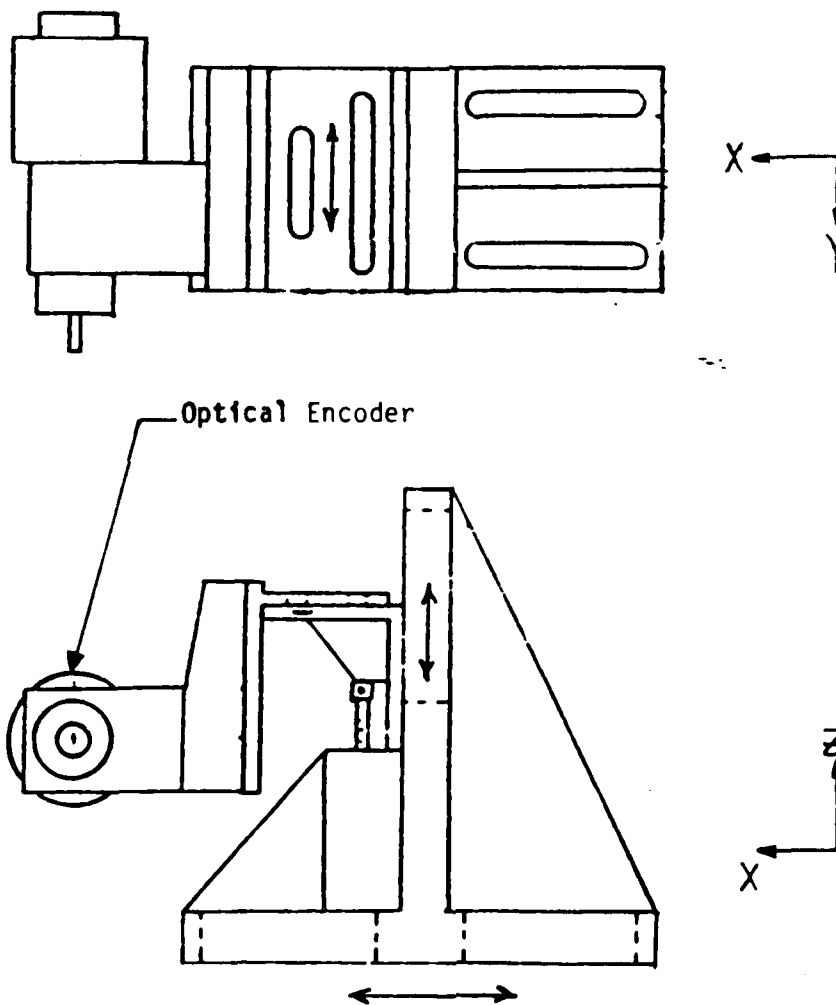


Figure 10: Mounting Bracket for the Optical Encoder

$$\omega_1 = 3.5 * 60 / N_p, \text{ rpm} \quad (3.1)$$

For the gear pair described in Chapter 1, which has 60 and 120 teeth (5 inch and 10 inch diameters and a diametral pitch of 12), the maximum pinion shaft speed would then be 3.5 rpm. This is an average size gear and for other gears the maximum pinion speed will range from 2-5 rpm.

The transmission error calculated by the signal processing unit is output on a strip chart recorder (an integral part of the processing unit) and as a voltage signal. Most of the controls of the unit (low pass and high pass filtering, chart scale, chart speed, etc.), affect only the transmission error plotted on the strip chart. A major drawback of this signal is that only the transmission error time domain plot is output, and it can only be examined visually. The output of transmission error as a voltage signal enables numerous post-processing capabilities. Some of the more useful capabilities are the spectral analysis of the transmission error, time averaging, enhanced graphics plotting, and the ability to store the data on disc for future analysis. Presently, a Wavetek 804A multi-channel Signal Processor is used in conjunction with a frequency divider and a proximity pickup to achieve the

above listed capabilities. The sampling rate of the gear is always synchronous with the gear rotation so exact harmonic orders of shaft speed are generated in the spectrum plot.

3.3 Test gear box

The test stand was designed to test gears that have parallel input and output shafts (primarily spur gears or helical gears). Due to the large transmitted forces the gear pair must be mounted in a gear box with bearings to withstand any axial or radial forces generated by the gear pair. This will improve the accuracy of the transmission error measurement by reducing the shaft deflections and will also decrease the loading on the drive source and load. Although it will be of interest to test gear pairs with different center distances, it is advisable to use a gear box with a fixed center distance rather a variable center distance since the radial shaft deflections are likely to be larger for the variable center distance gear box. A variety of gear boxes may be tested as the only physical restrictions are:

1. The gear box must have double-ended shafts so the optical encoders may be directly

connected.

2. The ground-to-shaft height for both gears must be the same and should not exceed the fixed height of the motor shafts, 20 inches.
3. The center distance must be at least seven inches to allow room for the optical encoders and the torquemeter. However, it is likely that more modern, miniaturized encoders will allow this dimension limit to be substantially reduced.

Although it would be convenient if the length of the overhanging shafts and the shaft diameters were identical for each gear box tested, it is not mandatory since the variations can be accounted for by different length connecting shafts between the gear box and the motor.

In order to raise the shaft height to the fixed centerline of the DC torque motors, the gear box will be mounted on a support fixture which, in turn, will be mounted to the base plate. In order to avoid having numerous mounting holes on the base plate surface, the support fixtures for all gear boxes should use the same mounting holes.

A gear ratio of two was used in designing the system for torque and speed levels, yet gear boxes with other gear ratios may be tested. In cases where the gear ratio is greater than two to one, the operating torque level will be limited by the maximum torque the

load motor can supply for the test time required.

3.4 Drive Source and Load Motor

The function of the drive motor is to supply the input torque and shaft speed to the gear box being tested. The peak torque rating of the drive source should be approximately 1,000 ft-lbf, while the speed is not a major concern since static transmission error is the primary measurement to be obtained and the Gleason/Goulder processing unit has a bandwidth of 11 Hz. However, moderate speeds are desirable in order to reduce data acquisition and signal processing time. Assuming some kind of motor and load torque ripple will be present, it would be preferred that the content be at high frequency, well above the mesh frequency if possible, so that its effects on the transmission error may be minimized by low pass filtering.

Three drive concepts, a DC torque motor, a hydraulic motor, and a four square rig, were investigated. Each apparatus has the capability of high torques.

A four square rig is a system which uses two gear pairs (either identical or have the same diameters and gear ratio) connected by two shafts in which the torque

is 'locked in' by fixing one side of a coupling on a shaft and rotating the other side of the coupling an initial angle before fastening. The induced torque is then equal to shaft stiffness multiplied by the angle displaced. Only a low powered motor (to overcome bearing and gear friction) is required to rotate the shaft, but the setup has a major drawback in that the slave gears have an undeterminable effect on the transmission error measurement and would have to be replaced for each gear box tested.

Two kinds of hydraulic motors, a screw type and a piston type, were analyzed, but both have minimum operating speeds well above the maximum test speed as governed by the processing unit. The screw type motor delivers smooth output torque, but has a minimum speed rating of about 1,000 rpm. Piston motors, will in general, operate continuously at 300 rpm, but have an objectionable ripple torque at a frequency from 8-11 per revolution (the number of pistons of the motor).

Each hydraulic motor would require a speed reducer, most likely a set of gears, because of their relatively poor performance at stall and slow speeds. Since the object of the test apparatus is measuring the positional accuracy of one set of gears, it was felt that

introducing another set of gears would harmfully affect this measurement and the torque transmitted. For this reason, along with the fact that hydraulic systems are often noisy and inherently messy due to leakage, the hydraulic motor as a drive source was deemed unacceptable.

The DC torque motor is a direct drive unit capable of maximum torque at zero speed (See Appendix A for operating characteristics of a DC torque motor). Although the maximum no load speed of a large torque motor is only 20-30 rpm, torques up to 2,000 ft-lbf are available for speeds from 5-10 rpm. The power input required by the motor is three phase which is usually supplied and regulated by a transformer and a DC servo amplifier/controller. The torque ripple of the motor is usually less than 4% of the mean torque and for large motors the torque ripple is around 200 times the shaft speed.

Even though the cost was somewhat higher compared to the other devices, the DC torque motor was selected for the drive source, since it can best provide the desired torque and speed levels with the smoothest operation, and can easily accommodate feedback controls. The feedback controls can allow for dynamic compensation

to essentially provide for the modification of effective shaft compliance and damping.

For the load brake, several devices seemed feasible to supply a resisting torque at low speeds. The devices considered were a DC torque motor, a hydraulic pump, an eddy current brake, and a disc brake. The hydraulic pump was discounted for the same reasons discussed earlier for the drive motor. Likewise, the eddy current brake does not operate well at or near stall conditions and would also require a speed increaser. Hence, it was also felt to be inadequate. The torque loading smoothness of the disc brake was questioned and its ability to apply rapid increases and decreases in torque for control purposes was felt to be inadequate. The DC torque motor, with the characteristics discussed above, again best satisfied the design requirements and was therefore selected as the load brake.

The test apparatus will, therefore, use a DC torque motor for both the drive motor and the load brake. It might be noted that these motors are the only type that are specifically designed to operate with a relatively high accuracy at low speed and high torque. Many of the other devices investigated are applicable to heavy duty equipment (trucks, prime movers, etc.) that are more

concerned with the nominal torque or nominal horsepower capability.

Several companies make DC torque motors, but few companies make torque motors with torque ratings of the magnitude desired in this test stand. The author could identify only two vendors, Inland Motor and Sierracin/Magnedyne, that make DC torque motors with torque ratings up to 2,000 ft-lbf. Both firms quoted DC torque motors for the drive source and the load brake, respectively. These motors were generally the same size with similar performance characteristics. The Sierracin/Magnedyne units had two outstanding characteristics which differ from the Inland units.

1. The magnets are made of Samarium Cobalt which has fewer operating and handling restrictions than the Alnico magnets in the Inland motors.
2. The cost of the drive and load DC torque motors are considerably less than the motors from Inland Motor.

On this basis, subsequent analyses are going to use the specifications of the Sierracin/Magnedyne torque motors. The chosen drive motor has a peak torque rating of 1,000 ft-lbf and a maximum no load speed of 30 rpm, while the load motor will be identical to the drive motor, but with "pushed" specifications per the vendor to allow operation at a peak torque of 1,600 ft-lbf. A second

motor which has a peak torque rating of 2,000 ft-lbf and a maximum no load speed of 15 rpm could also be used.

Typically, DC torque motors are marketed without a housing or a shaft (frameless) so that they can be designed as an integral part of the system hardware. For the transmission error measurement application the following modifications are needed:

1. Addition of an end bell equipped with bearings to support the shaft for each motor. Electrical connections should be provided on one of the end bells.
2. A shaft attached to the armature which extends through both end bells (one for the gear box and one for a tachometer).
3. A support structure to mount the torque motors on the bedplate. The shafts must be horizontal and each motor must have the same shaft height.

Bids to design, machine, and assemble the housings have been requested from three companies. Of the two preliminary designs received, one uses a flange mount, while the other uses a foot mount. Both designs seem adequate and include the features listed above.

3.5 Feedback Transducers

Both speed and torque are to be controlled during the test, with torque being the primary control variable because transmission error is a function of the relative angular position of the gears rather than the instantaneous angular velocity. The modeling process to be discussed in Chapter 4, however, shows that speed feedback is needed for each motor in order to increase the stability of the closed loop response since the DC torque motors and the test gear box have very little mechanical damping.

Since the test speeds will be in the range of 2-5 rpm, it would be preferred that the speed be measured with an optical encoder rather than a tachometer generator for the latter have low frequency ripple voltages that might disturb the transmission error measurement and they also typically have relatively low voltage outputs at the low speeds. In order to convert the pulse train output of the encoder to a voltage signal required by the DC controller, a frequency-to-voltage converter will be required.

It will be shown in Chapter 4 that the speed may be measured anywhere along the shaft with similar results. Therefore, an accessible and convenient location for the

speed pickup is on the side of the torque motor opposite to the gear box. In order to accommodate the encoders, the torque motors will have double-ended shafts so that the encoders can be attached to the motor housing by a flange mount and secured to the shaft with a setscrew or a keyway.

From the analysis of Chapter 4, torque control was equally achieved when the torque was measured on either the low or high torque shaft. In order to have the option of measuring the torque on either shaft, the torquemeter selected has a capacity of 1,670 ft-lbf, but is overloads protected to up to 2,500 ft-lbf. The slip ring torque sensor was chosen to have a flange mount, rather than a shaft drive, because this is the best means of minimizing shafting length and couplings between the gear mesh and the torque measurement torque so that the measured dynamic torque is identical as possible with the torque on the test gear pair. Additionally, the number of couplings required on the load shaft is then reduced from three to two. There is no support base for the torquemeter, but a restraining strap is attached to it and the base plate to keep it from rotating. The torquemeter is externally excited by a DC strain gage signal conditioner and amplifier.

3.6 Motor Controller and Amplifier

A DC servo amplifier/controller generates an error signal by summing the command input(s) and the feedback input(s) (which should be of opposite polarity), then amplifies the error to increase or decrease the current delivered to the motor. One controller is required for each motor. The controller for the drive motor will control on drive motor shaft speed, while the controller for the load motor will have a command and feedback input of load torque plus a second feedback input of load shaft speed in order to enhance the system damping.

The same controller, Glentek model GA4580, was selected for each motor. In addition to the self protection circuits of the controller, the Glentek controller has following features:

1. Two command or feedback inputs plus a tachometer feedback input.
2. Current may be limited for peak value and can also be tapered as a function of velocity.
3. Current control.
4. CW, CCW, or CW and CCW drive inhibitors.

To avoid overheating of the motor armatures a thermostat attached to the armature which produces an on-off signal will be input to the controllers' "inhibit both

directions" input to shut down the motor when in the 'on' state.

Each controller requires three phase power for the main power to the DC motors and 120V single phase power to drive the fans, logic circuits, etc. A transformer is required to drop down the available 208VAC three phase voltage to a level in the range of the operating voltage, about 30VAC. Glentek markets a transformer, model T345, which will accept the primary voltage of 208V and output a secondary voltage of 70V. Although the secondary voltage level is higher than the operating voltage, it is acceptable. The unit will also output 120V single phase power. One transformer can service both controllers if it is of sufficient capacity, otherwise one transformer is required for each controller.

3.7 Couplings and Spacers

Connecting the torque motors to the gear box will require one full coupling and one spacer for each motor. The spacer for the load motor, in addition to matching the couplings, must also match up with the torquemeter. In general, the spacers and couplings will be unique to each gear box and will have to be purchased accordingly.

The optical encoders will be linked to the gear box by high precision, flexible couplings. Again, these couplings will be specific to the gear box and will be purchased accordingly.

3.8 Base Plate

The base plate provides for a common, level mounting surface for the test stand equipment. It measures five feet wide, nine and one half feet long, six inches high, and weighs approximately 4,600 lbs.

The transmissibility of vibrations from the test stand to the ground is not of major concern since any vibration frequencies will be very low. However, the base plate will rest on rubber pads in order to partially correct for the unevenness of the floor, and the asymmetric loading of weight on the base plate. Six pads are to be used: one for each of the four base plate support fixtures which measure six by ten inches, and two under the five inch wide support plate which spans the width of the base plate. The anticipated weight of the test apparatus, including the weight of the base plate, is 7,500 lbs. Therefore, the average weight on each pad would be 1,250 lbs. which is within the recommended range of the minimum and maximum load for

the pad.

3.9 Installation of Equipment

A design consideration of the system was the interchangeability of gear boxes that results in the fewest modifications to other system components. In general, each gear box will have a different ground-to-shaft height, different shaft diameters, different length of overhanging shafts, and different center distances. As previously noted throughout this chapter, most of the adjustments will be made by changing the gear box support fixture, couplings, and spacers for each gear box tested. The changes required to test a new gear box are as follows:

1. The height, and therefore the support structures, of both DC torque motors and encoders will remain fixed by supporting the gear box with a fixture to raise it to the height of the motor shafts.
2. The different shaft diameters will be accounted for by changing the flexible couplings of the encoders and changing the half couplings to the torquemeter and to the drive shaft.
3. The various lengths of the gear box shafts will be accommodated by using different length coupling spacers and different flexible couplings to the encoders.
4. The change in center distance requires the

most modifications; one DC torque motor and the optical encoder connected to that shaft must be moved laterally. By outfitting the foot mounts for the motor and encoder with slots, no new holes will need to be drilled into the base plate for small changes in the center distance.

The final design layout of the system is shown in Figure 11.

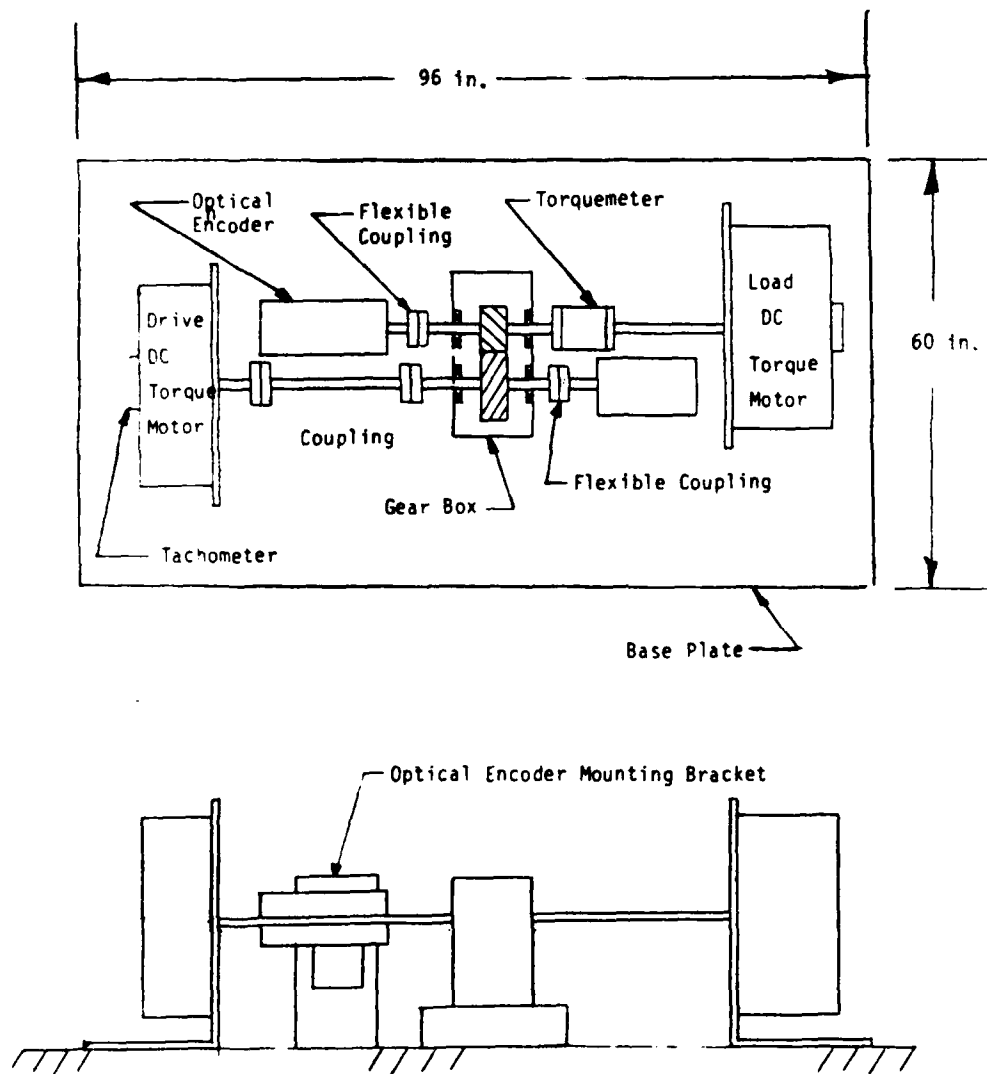


Figure 11: System Layout

Chapter 4

DYNAMIC MODELING AND RESPONSE

4.1 Introduction

In order to isolate the transmission error of the gear pair, it is desired to maintain the torque and speed at a steady value throughout a test. Variations in torque are more harmful than speed variations as they will cause the gear tooth deflections to fluctuate, which will result in an error in the transmission error measurement. Since transmission error is a function of relative angular displacement, speed changes will only be a problem if they are too fast for the data sampling unit to follow.

In addition to the control of torque and speed the influence of the environment on the measurement of transmission error should be minimized. In order to achieve these performance goals the following design criteria were emphasized.

1. System natural frequencies should be at least 5 times the third harmonic of mesh frequency. Since the test speed will often be run at

maximum speed, the third harmonic of mesh frequency will be about 11 Hz (70 rad/sec) as limited by the processing unit. Hence, system torsional natural frequencies should be at least 55 Hz (345 rad/sec).

2. The damping ratio, ζ , should be at about 0.6 to 0.7 if possible, to decrease the settling time of command and transient inputs.
3. The disturbance inputs, such as torque motor ripple or transmission error, should have a minimum effect on the torque transmitted by the gears.

Since few physical parameters can easily be changed once the torque motors are selected, any system characteristic requiring modification will need to be implemented by the control regime which is used. This chapter discusses the control method that will be used to achieve the performance requirements stated above. The nomenclature used in this chapter are listed in Table 1.

4.2 Dynamic Model and Equations

Figure 12 shows a model of the system including only the torsional degrees of freedom. For convenience, the system was analyzed in three separate free-body diagrams.

1. Drive motor shaft and electric circuit.
2. Pinion to gear interaction.

Table 1: Nomenclature

K_a = DC torque motor torque gain per input voltage
 K_b = DC torque motor back emf constant
 τ_a = DC torque motor electrical time constant
 K_1 = drive motor proportional gain of drive motor speed
 K_2 = drive motor proportional gain of pinion torque
 K_3 = load motor proportional gain of pinion torque
 K_4 = load motor proportional gain of load motor speed
 τ_1 = drive motor derivative gain of drive motor speed
 τ_2 = drive motor derivative gain of pinion torque
 τ_3 = load motor derivative gain of pinion torque
 τ_4 = load motor derivative gain of load motor speed
 J = mass moment of inertia of the DC torque motor
 K = effective shaft stiffness
 n = gear ratio
 TE = transmission error
 T_d = desired pinion torque input
 T_p = pinion torque
 ω_d = desired drive motor shaft speed
 ω_1 = drive motor shaft speed
 ω_2 = load motor shaft speed
 R_p = pinion radius
 R_g = gear radius
 E_1 = input voltage to the drive motor
 E_2 = input voltage to the load motor

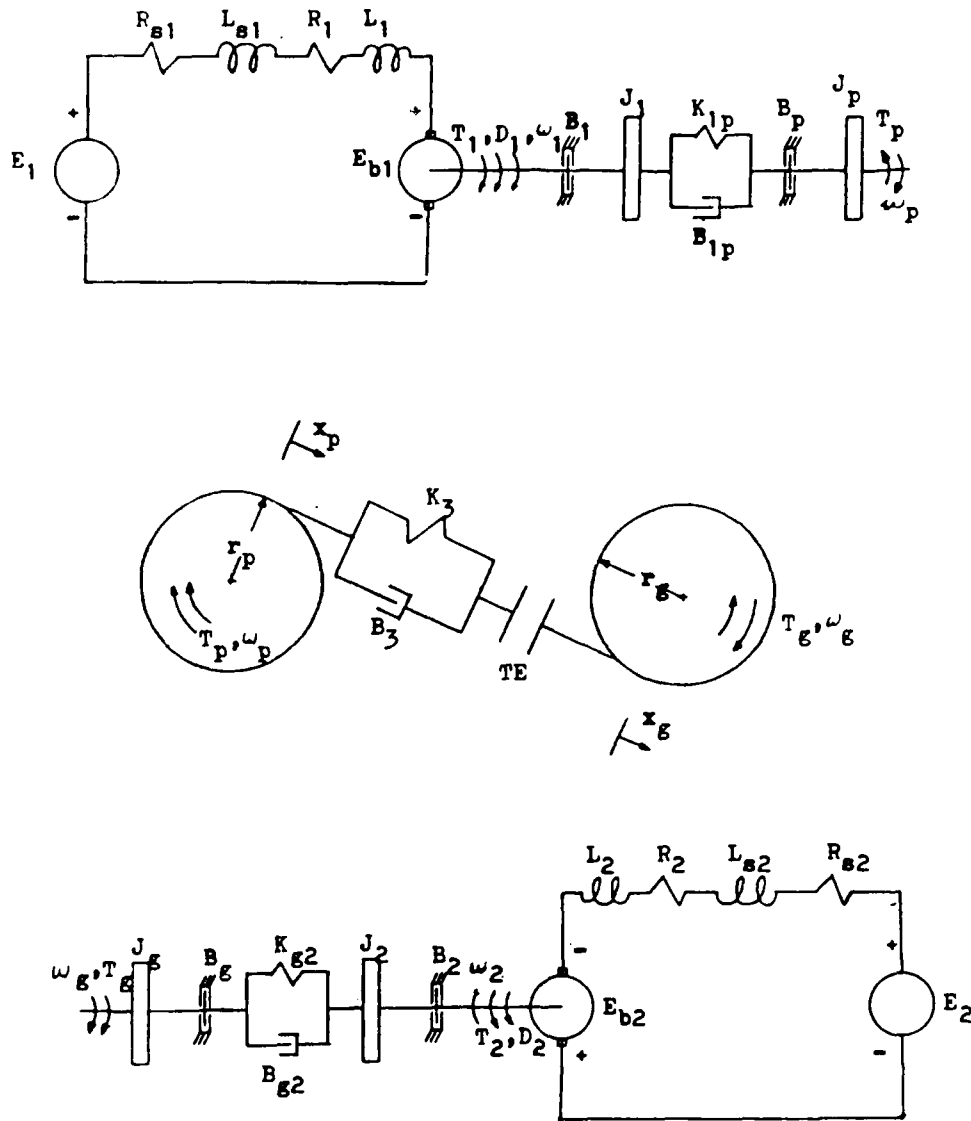


Figure 12: Physical Model of the Dynamic System.

3. Load motor shaft and electric circuit.

Disturbance inputs have been included to see how the system would react to any other physical or hypothetical disturbance. Three disturbances were selected: drive motor ripple torque (D_1), transmission error (TE), and load motor ripple torque (D_2).

From the model in Figure 12 the dynamic equations may be written using Kirchoff's voltage loop law and Newton's second law of motion. The equations are written below assume the two DC torque motors have different specifications.

$$\begin{aligned}
 0 &= E_1 - I_1(s(L_1 + L_{s1}) + R_1 + R_{s1}) - E_{b1} \\
 J_1 s \omega_1 &= T_1 + D_1 - B_1 \omega_1 - B_{1p}(\omega_1 - \omega_p) - K_{1p}(\theta_1 - \theta_p) \\
 J_p s \omega_p &= K_{1p}(\theta_1 - \theta_p) + B_{1p}(\omega_1 - \omega_p) - B_p \omega_p - T_p \\
 T_p &= R_p(sB_3 + K_3)(R_p \theta_p - R_g \theta_g + TE) \\
 T_g &= R_g(sB_3 + K_3)(R_p \theta_p - R_g \theta_g + TE) \\
 J_g s \omega_g &= T_g - B_g \omega_g - B_{g2}(\omega_g - \omega_2) - K_{g2}(\theta_g - n\theta_2) \\
 J_2 s \omega_2 &= K_{g2}(\theta_g - \theta_2) + B_{g2}(\omega_g - \omega_2) - B_2 \omega_2 - T_2 - D_2 \\
 0 &= E_2 - I_2(s(L_2 + L_{s2}) + R_2 + R_{s2}) + E_{b2}
 \end{aligned}$$

For a permanent magnet DC torque motor, the torque developed is proportional to the current and the back emf is proportional to the angular velocity. This

proportionality constant can be shown [4] to be identical for both equations, but is usually expressed in different, but compatible units.

$$T_1 = K_{t1} I_1$$

$$E_{b1} = K_{b1} \omega_1$$

$$T_2 = K_{t2} I_2$$

$$E_{b2} = K_{b2} \omega_2$$

To complete the set of equations, a relationship of the radius at the point of contact is needed. It is assumed that the point of contact is on the line of action, hence, the gear ratio is constant.

$$n = \frac{R_g}{R_p}$$

Although the math model includes elements that will be present in the physical system, reasonably good assumptions may be used to eliminate some elements which will reduce the complexity of the model without sacrificing any loss of model accuracy. The following elements were judged to have minimal influence on the system.

1. The power source inductances are negligible relative to the armature inductance of the DC torque motors.
2. The viscous damping coefficients of the

motors are less than 1 ft-lbf/(rad/sec) and the maximum test speed will be less than 1 rad/sec. Therefore, the damping torque will be less than 1 ft-lbf. Since the typical shaft torque will range from 700 to 1400 ft-lbf, the damping torque will be negligible. Damping coefficients of the shafts, gears, and gear teeth were estimated to be less than the torque motor damping, hence, they were also felt to be negligible. Therefore, all of the mechanical damping terms were neglected.

3. The mass moment of inertias of the pinion and of the gear were calculated to be less than 2 percent of the mass moment of inertia of the DC torque motors for the largest gears expected to be tested. It was assumed that the energy required to accelerate or decelerate the gear inertias to be small compared to the energy stored in the shaft of DC torque motors. Likewise, typical torsional natural frequencies of gear-pinion pairs are in the 1,000 Hz to 4,000 Hz range which is well beyond the frequencies of concern in this analysis.

It should not be surprising that the mechanical damping terms were small since the gears are lightly damped and the function of the torque motor is to provide torque rather than to dissipate it through heat. Eliminating these elements, combined with the fact that both motors have identical parameters, considerably reduced the complexity of the system as shown in Figure 13. The simplified block diagram of the system is shown in Figure 14.

All of the following analyses will use the specifications of the gear pair previously stated in

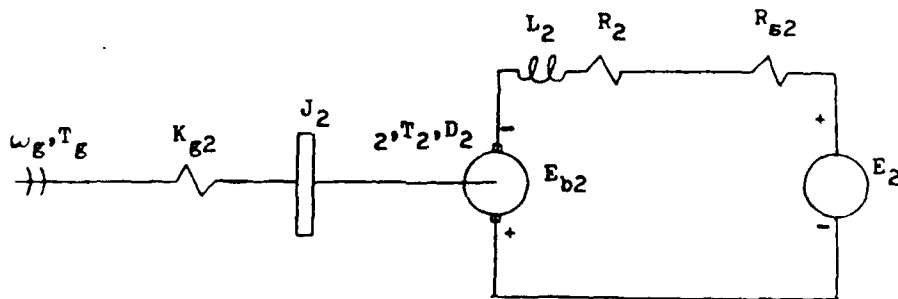
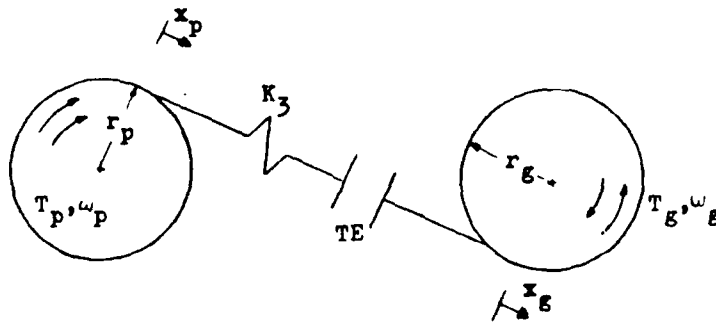
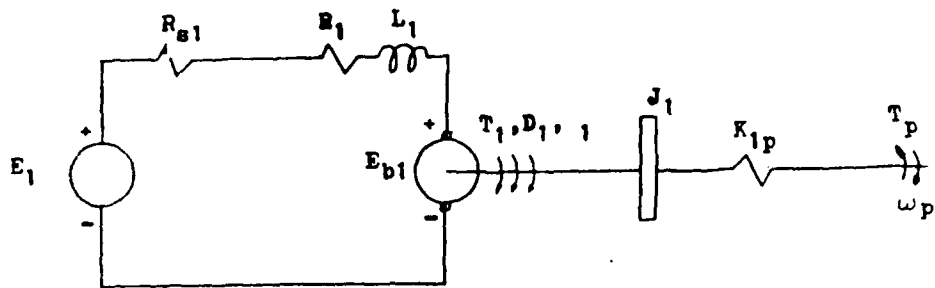


Figure 13: Simplified Physical Model of the Dynamic System

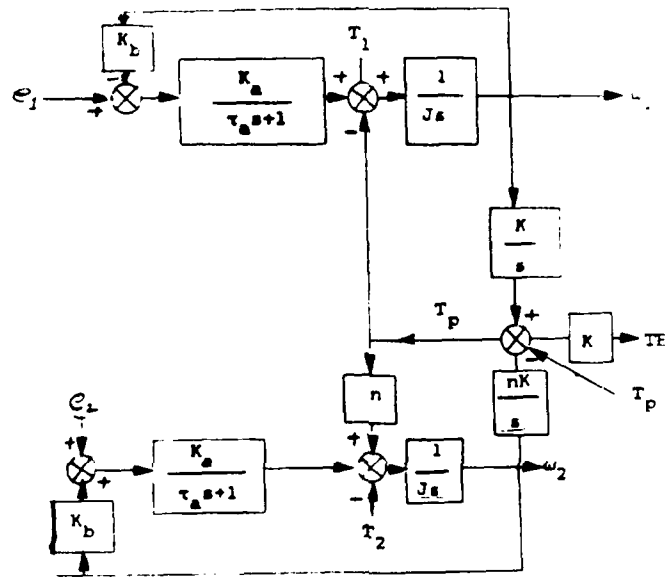


Figure 14: Open Loop Block Diagram of Simplified System

Table 2: Sample Gear Specifications

7.5 inch	Center Distance
5.0 inch	Pinion Diameter
10.0 inch	Gear Diameter
2.5 inch	Face Width
2:1	Gear Ratio
12	Diametral Pitch
60	Pinion Teeth
120	Gear Teeth

Chapter 1. The specifications are restated in Table 2.

4.3 Open Loop Response

Since the system is fifth order, a closed-loop solution of the transfer functions in factored form is not possible. Therefore, other numerical methods were used. One such method, through the use of a digital simulation program (ACSL, Advanced Continuous Simulation Language) uses a numerical integration technique (Runge-Kutta) to solve differential equations digitally. By calculating the response of the system numerically, numerous non-linearities can be introduced into the system. One such non-linearity is the saturation limit

of the DC torque motor and the DC servo controller. The saturation limit of voltage and current were implemented with IF statements (IF (I .GT. 100)I = 100) and limited to 100 volts and 100 amps, respectively. The program was used to observe the time response of the shaft torque and motor speeds to a step voltage input applied at either or both motor(s). The time trace quickly and easily shows the speed of response and allows the approximation of the damping ratios.

A step voltage input was applied to one motor (the responses were nearly the same when applied to either motor) and the plot of torque and drive motor speed were plotted versus time as shown in Figure 15. By measuring the period of the oscillations, the dominant natural frequency was approximated to be about 18 Hz (113 rad/sec). Clearly, the system is underdamped, but the damping ratio can only be estimated from the plot.

In order to numerically obtain the damping ratios and corresponding natural frequencies, the transfer functions were solved in letter form from a five by five matrix of the system equations. Calculation was greatly simplified by first reducing the rank of the matrix to two. Both motor currents and the load motor speed terms were eliminated since the pinion torque and drive motor

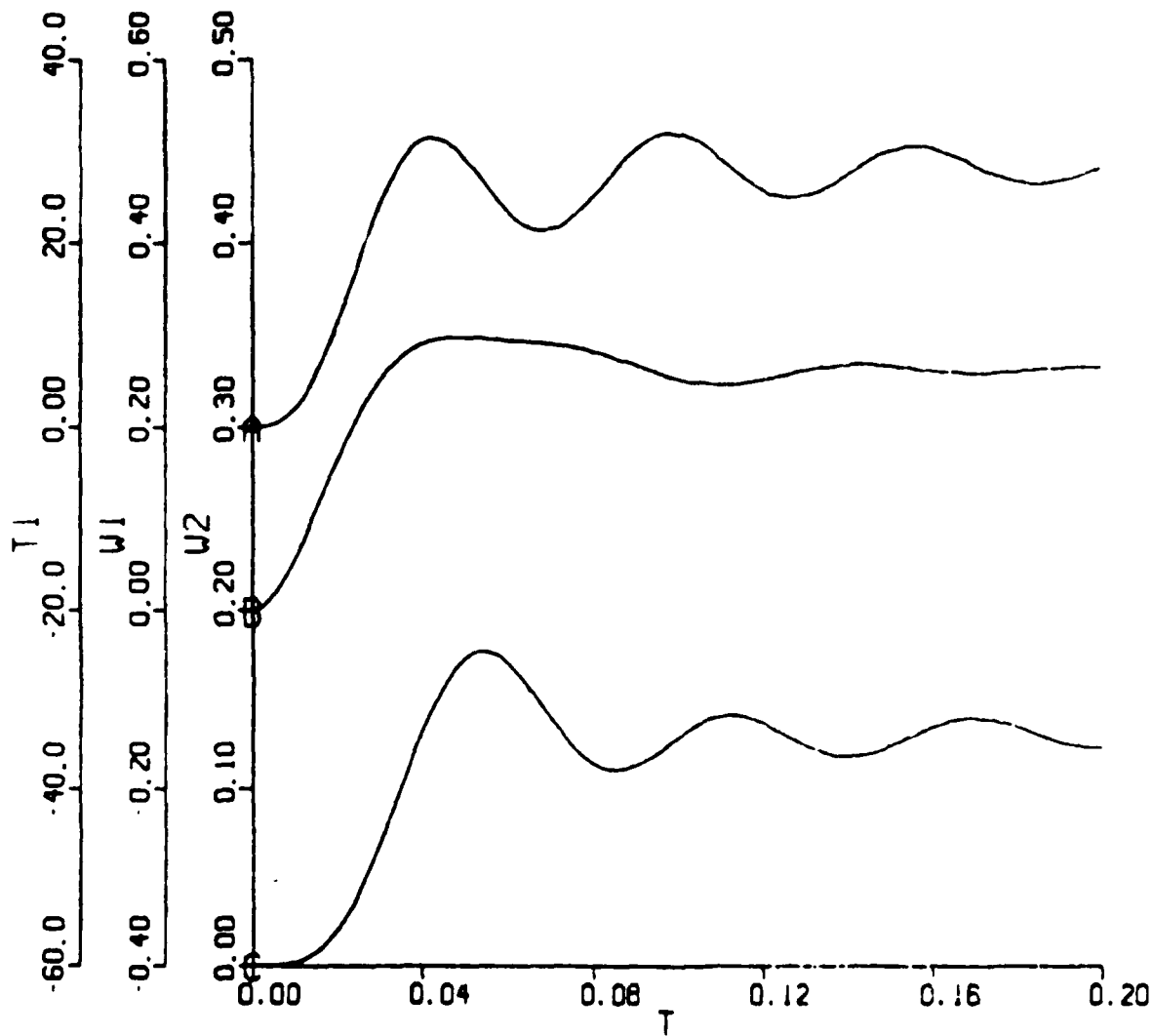


Figure 15: Open Loop Pinion Torque and Shaft Speed Responses for a Step Voltage Input

speed were of primary interest. In reducing the matrix the variables could have been eliminated (one by one) by substitution, but rederiving the equations from the block diagram of Figure 14 was found to be a simpler method. The numerator was second or third order and was easily factored. The denominator which is the characteristic equation was fifth order which required a root-finding program in order to determine the factored form.

The transfer functions obtained are displayed in a conventional dual input/dual output (drive motor and load motor supply voltage / pinion torque and drive motor shaft speed) shown in Figure 16. In addition to the natural frequency of 17.3 Hz (109 rad/sec) seen in the time domain (with a damping ratio of .09), a second pair of complex roots and a real pole are shown.

A Bode plot of the transfer function of pinion torque output for a sinusoidal voltage input was graphed with a matrix frequency response computer program and is shown in Figure 17. The frequency response plot correlates with the other two analyses in that they have similar natural frequencies and about the same damping ratios. Only two decades of frequencies are plotted (from 1 Hz to 100 Hz) since the plots approach

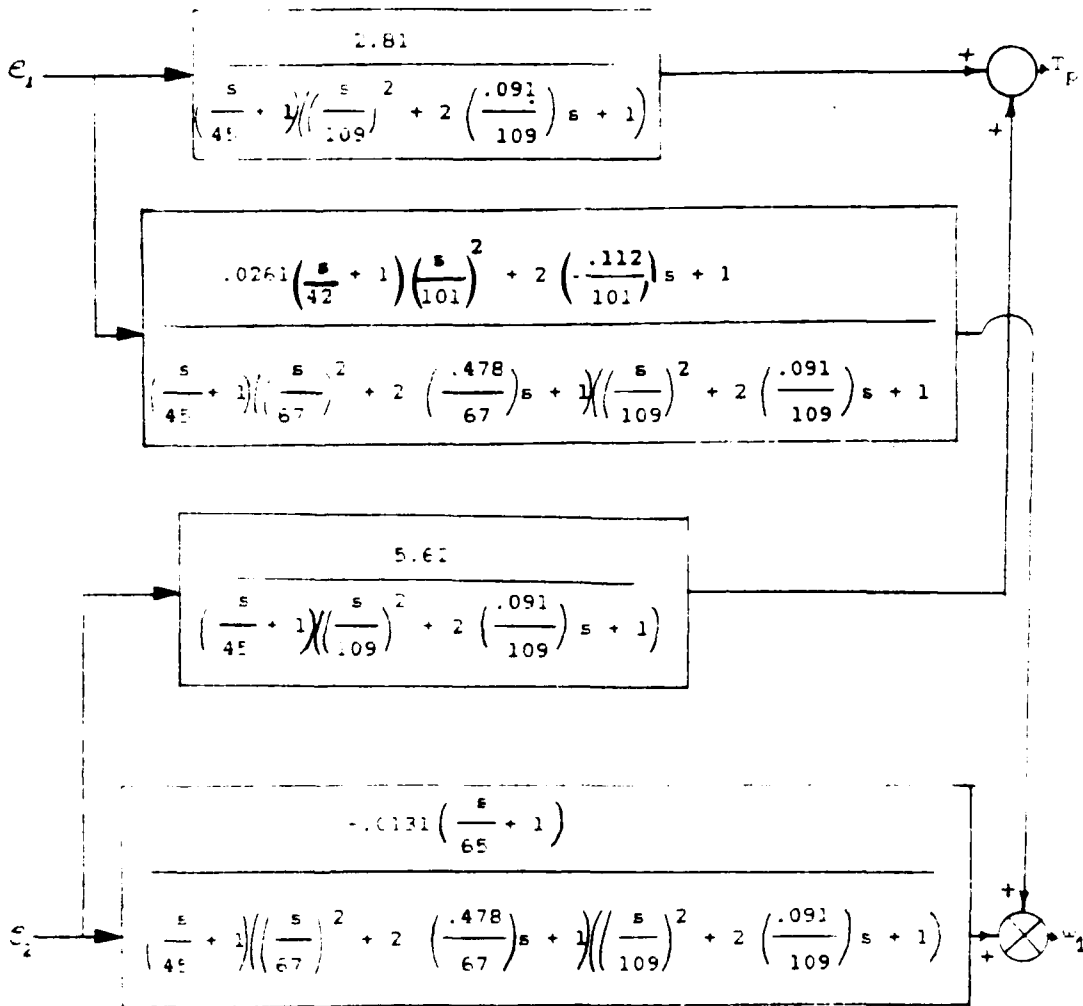


Figure 16: Open Loop Transfer Functions for the Dual Input/Dual Output Block Diagram

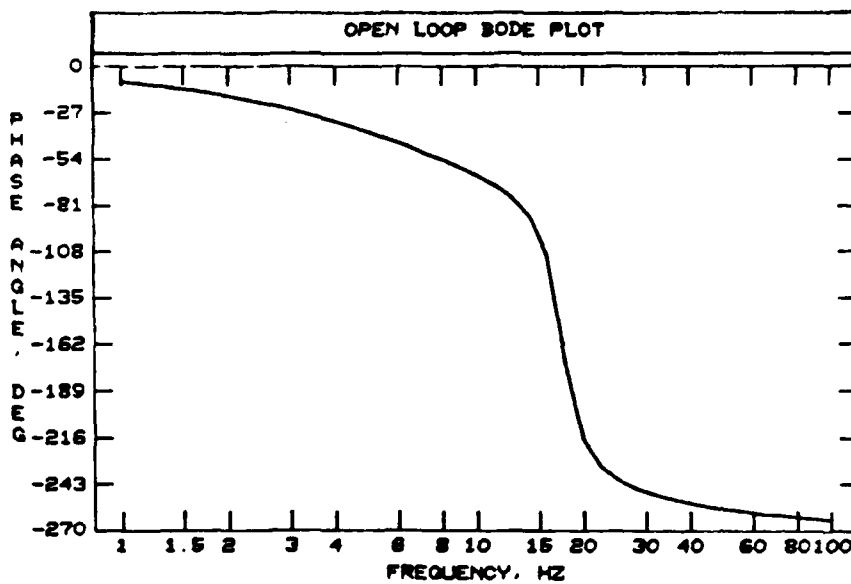
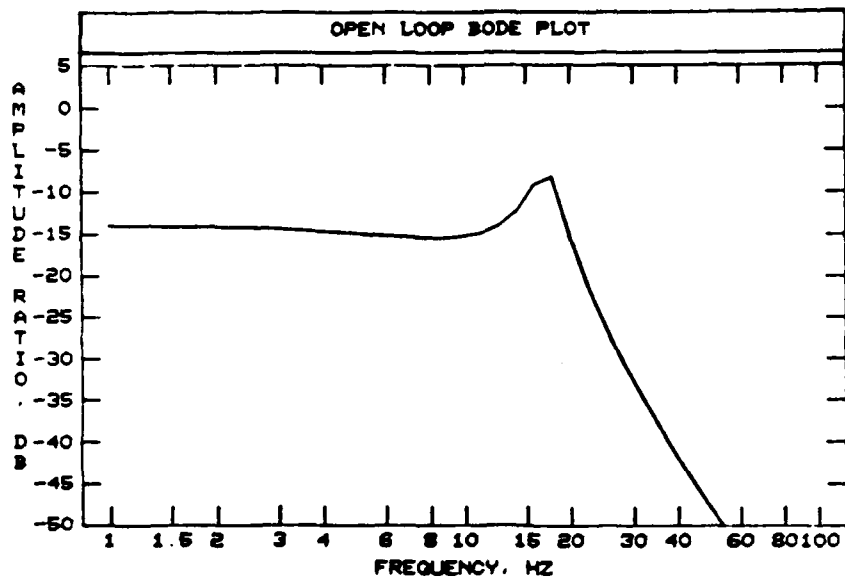


Figure 17: Open Loop Bode Plot of Pinion Torque Output for an Sinusoidal Input Voltage

asymptotes for frequencies less than 1 Hz and above 100 Hz, respectively.

The transfer functions of pinion torque output for each disturbance input were plotted in Figures 18 and 19. Indicated on the respective plots are the motor ripple torques and a transmission error component at mesh frequency. Ideally, the output pinion torque for a disturbance torque input would be zero, but both torque disturbances are seen to modulate the output torque by .4 ft-lbf per 1. ft-lbf of disturbance torque input for frequencies less than 40 Hz.

The transmission error input was originally in the units of feet. Since a foot of transmission error is very unreasonable, the units were converted to an input of .001 inch. The maximum amplitude occurred at the resonance and was .05 ft-lbf per .001 inch input. Slightly away from the resonance frequency, the amplitude ratio decreased considerably to less than .001 ft-lbf. Hence, unless the transmission error contained content at the natural frequency, its effect on the transmitted torque would be negligible.

From the list of design criteria, the open loop system was deficient in all of the categories in that both natural frequencies were well below 55 Hz (345

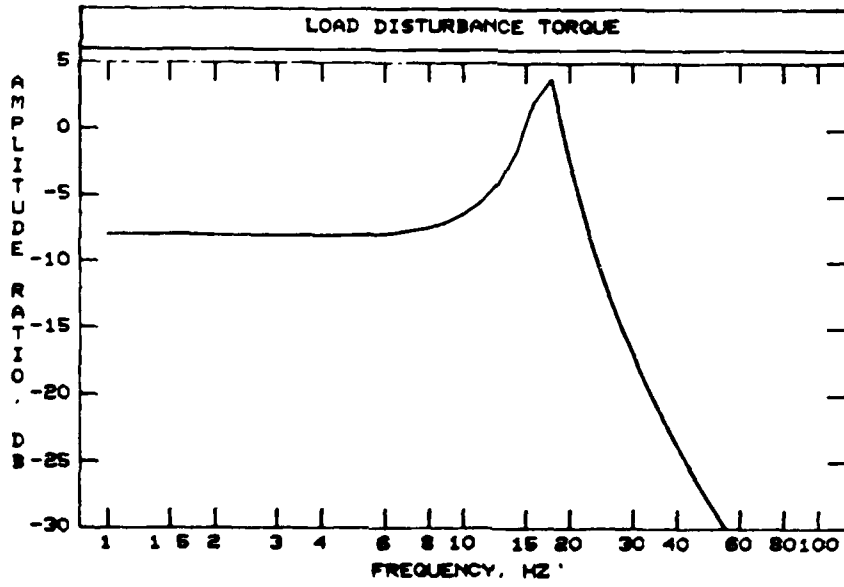
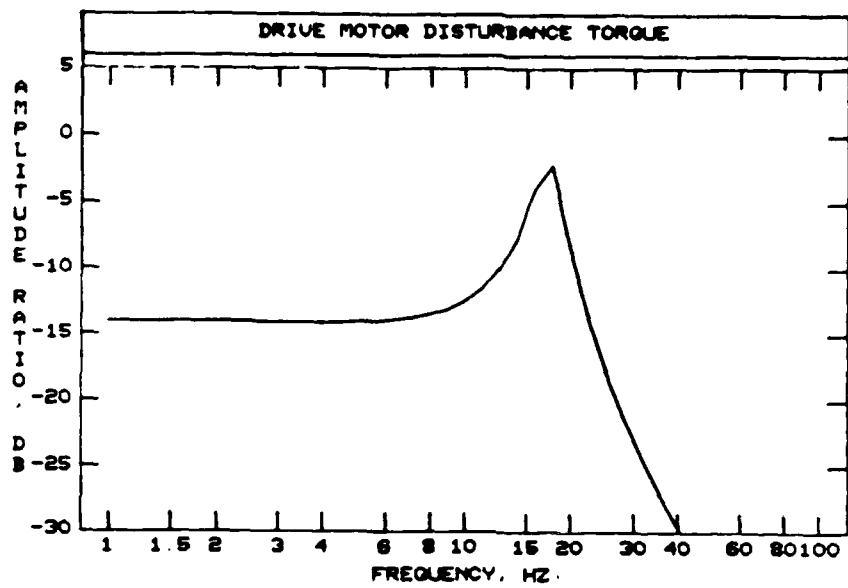


Figure 18: Open Loop Bode Plot of Pinion Torque Output for a Sinusoidal Disturbance Torque Input

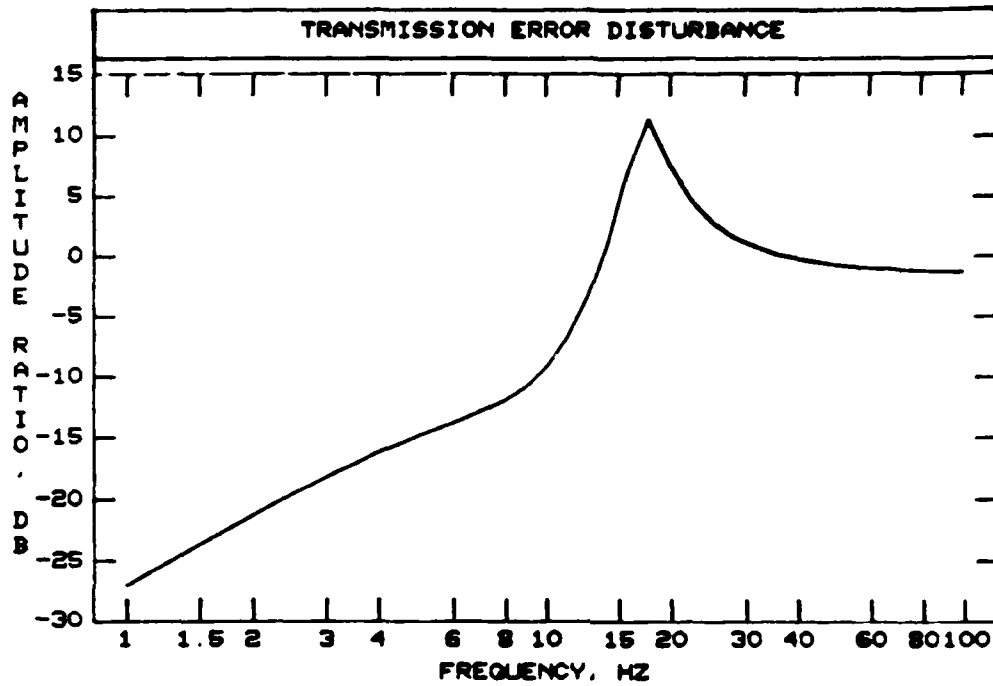


Figure 19: Open Loop Bode Plot of Pinion Torque Output for a Sinusoidal Disturbance Input of Transmission Error

rad/sec), one damping ratio was very low (.09), and the system offered only a 40% reduction of disturbance torques. Therefore, the open loop system is unacceptable and a feedback control system is needed.

Before proceeding with the feedback control analysis, the system was inspected for further possible simplifications. The electrical inductances could not be neglected as the resulting characteristic equation did not have the low damped second order root. The gear shaft was assumed to be of infinite stiffness, but the system was overly simplified with no second order terms (no complex roots). Additionally, different gear ratios were tested, but the characteristic equation was found to be independent on the gear ratio since only the gain of the input voltage was affected.

4.4 Proportional Control

Two command inputs, pinion torque and pinion speed, and three feedback signals, pinion torque, drive motor shaft speed, and load motor shaft speed, were implemented. For generality, both command inputs were input to each motor. In practice, there will only be pinion torque command input to one motor and pinion speed command to the other motor. The command signals

will not alter the system characteristic equation, but will affect the steady state values of torque and speed.

Since it was assumed that the torque ratio is constant, the torquemeter (for analysis purposes) may be placed on either shaft of the gearbox and its feedback signal may be input to either the drive motor or the load motor. Intuitively, the speed signal should be measured on the shaft for which it will be used as a feedback signal and hence, it will be simulated to be measured on the shaft of the drive motor or load motor inertia as required.

The block diagram of Figure 14 was then modified to include the command inputs and feedback signals stated above using proportional control as shown in Figure 20.

The controller gains are stated below:

K_1 = drive motor speed proportional gain

K_2 = drive motor torque proportional gain

K_3 = load motor speed proportional gain

K_4 = load motor torque proportional gain

Initially each gain was varied while the other three gains were set to zero in order to observe single loop control. For nearly all values of drive motor torque gain, K_2 , the system was found to be unstable. Similarly, with K_1 , K_3 , and K_4 set to zero, the system

was found to be unstable for nearly all values of load motor torque gain, K_3 .

By contrast, for all values of drive motor speed feedback gain, K_1 , with K_2 , K_3 , and K_4 set to zero, or for all values of load motor speed gain, K_4 , with K_1 , K_2 , and K_3 set to zero, the system was stable. The coupling between the drive motor speed and the load motor speed was relatively small as the controlled speed had good response time with little damping, while the torque response and the speed response of the uncontrolled motor had more damping, but were still slightly oscillatory as shown in Figure 21. The responses were similar when the feedback signal was applied to either motor.

Several combinations of torque and speed control were simulated. The use of torque control provided stability only when accompanied by speed feedback of the torque controlled motor. Therefore, drive motor speed gain, K_1 , was needed when drive motor torque control, K_2 , was used and load motor speed gain, K_4 , was needed when load motor torque control, K_3 , was used. At larger torque gains, the response time for torque was improved, but the lack of damping led to near marginal stability as shown in Figure 22. The response was similar for

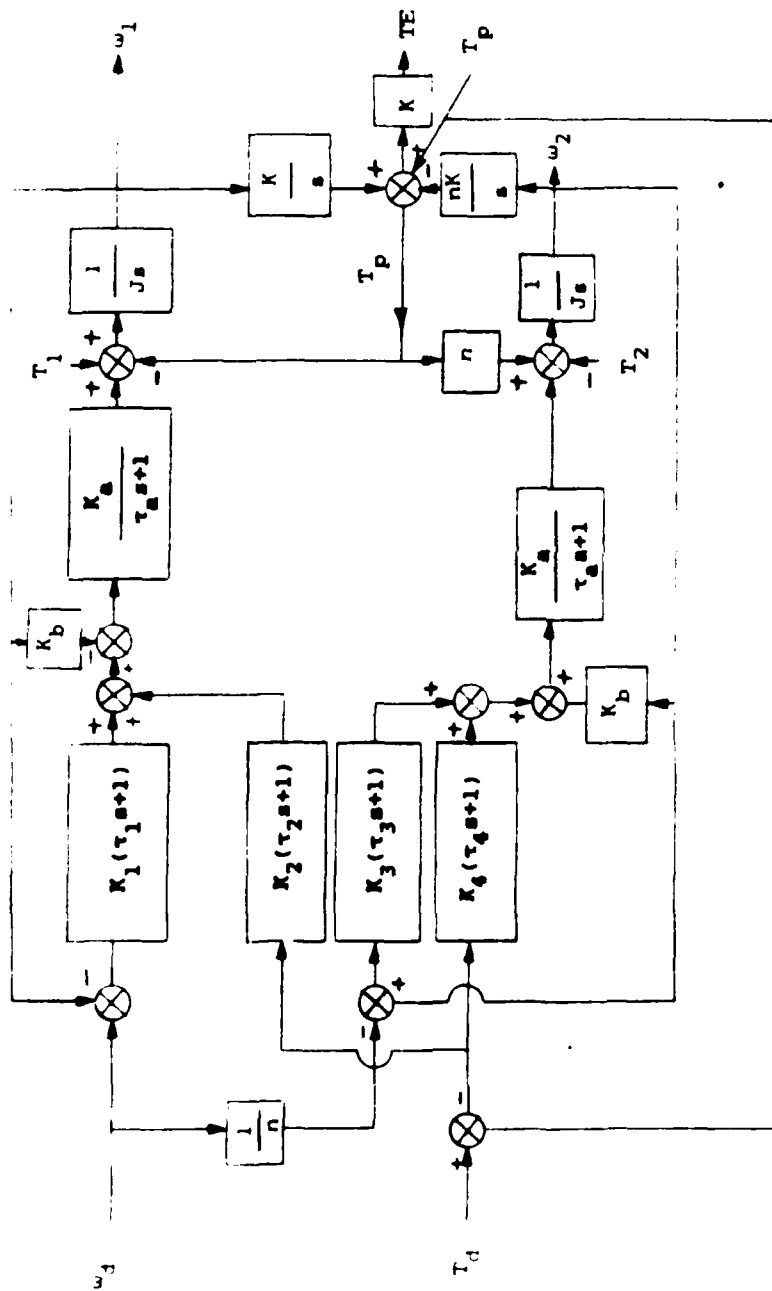


Figure 20: Closed Loop Block Diagram with Partial Control

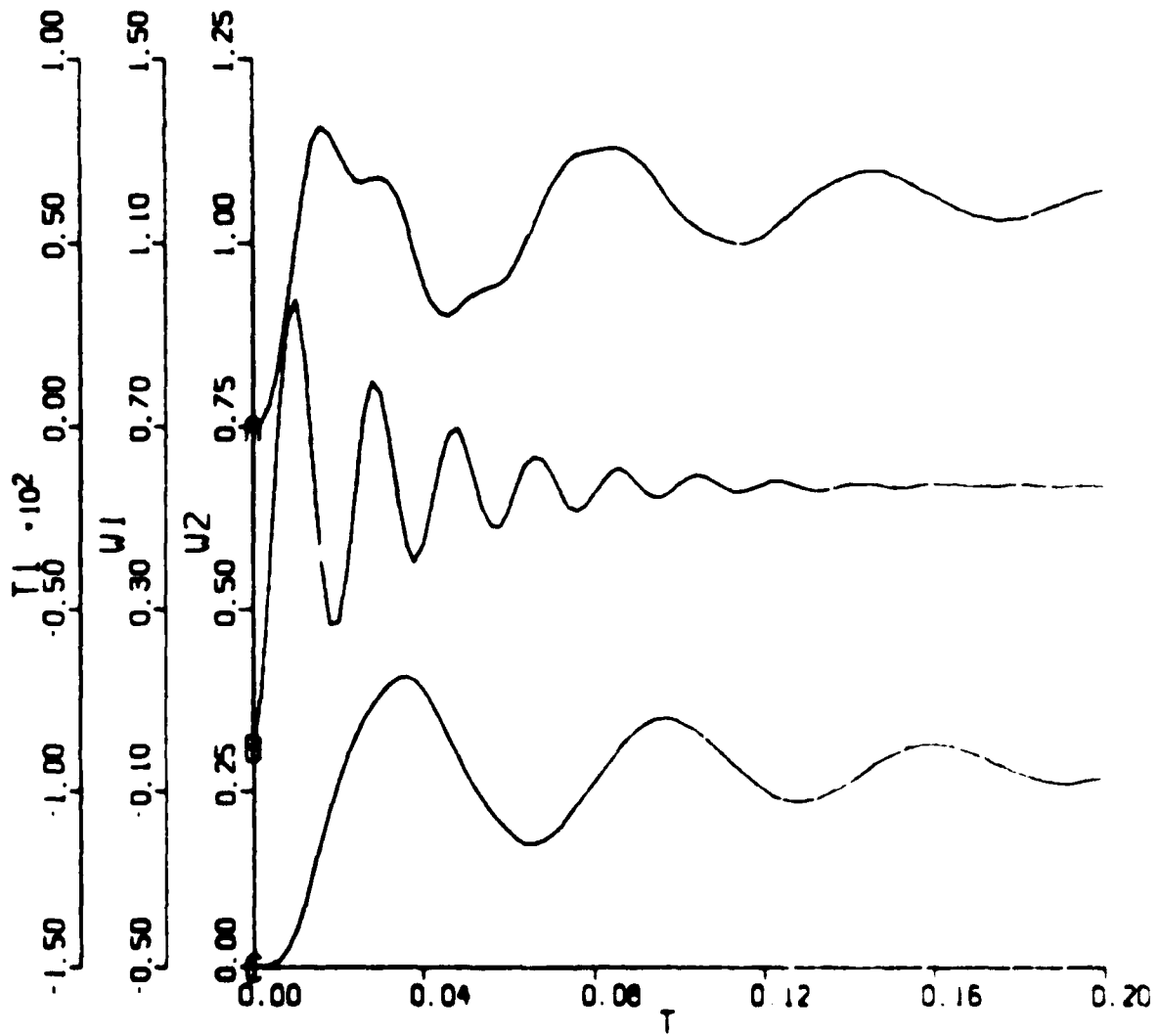


Figure 21: Pinion Torque and Motor Speed response for Proportional Speed Control of Drive Motor

either motor.

As a case of interest, both speeds were fed back without any torque feedback. Without a torque error signal the torque transmitted was nil as both motors were content only to rotate themselves, but the end effect of the combined speed feedbacks was approximately the combined effect of their individual use. Both shaft speeds were underdamped with higher natural frequencies which were identical for a gear ratio of one.

Combining torque control, K_2 or K_3 , with both of the shaft speed control loops, K_1 and K_4 , only marginally improved the torque response as shown in Figure 23. A similar response was obtained when the torque feedback was applied to either motor, except the gain of each motor needed to be scaled differently for each gear ratio in order to obtain a similar response. (The torque gain of the drive motor, K_2 , was set equal to the gain of the load motor, K_3 , multiplied by the gear ratio). When torque feedback was applied to both motors, K_2 and K_3 with K_1 and K_4 , the torque response was nearly the same as with a single feedback input, except that the torque oscillations were slightly larger. For a gear ratio of unity, the motor speed responses were identical for the same speed and torque

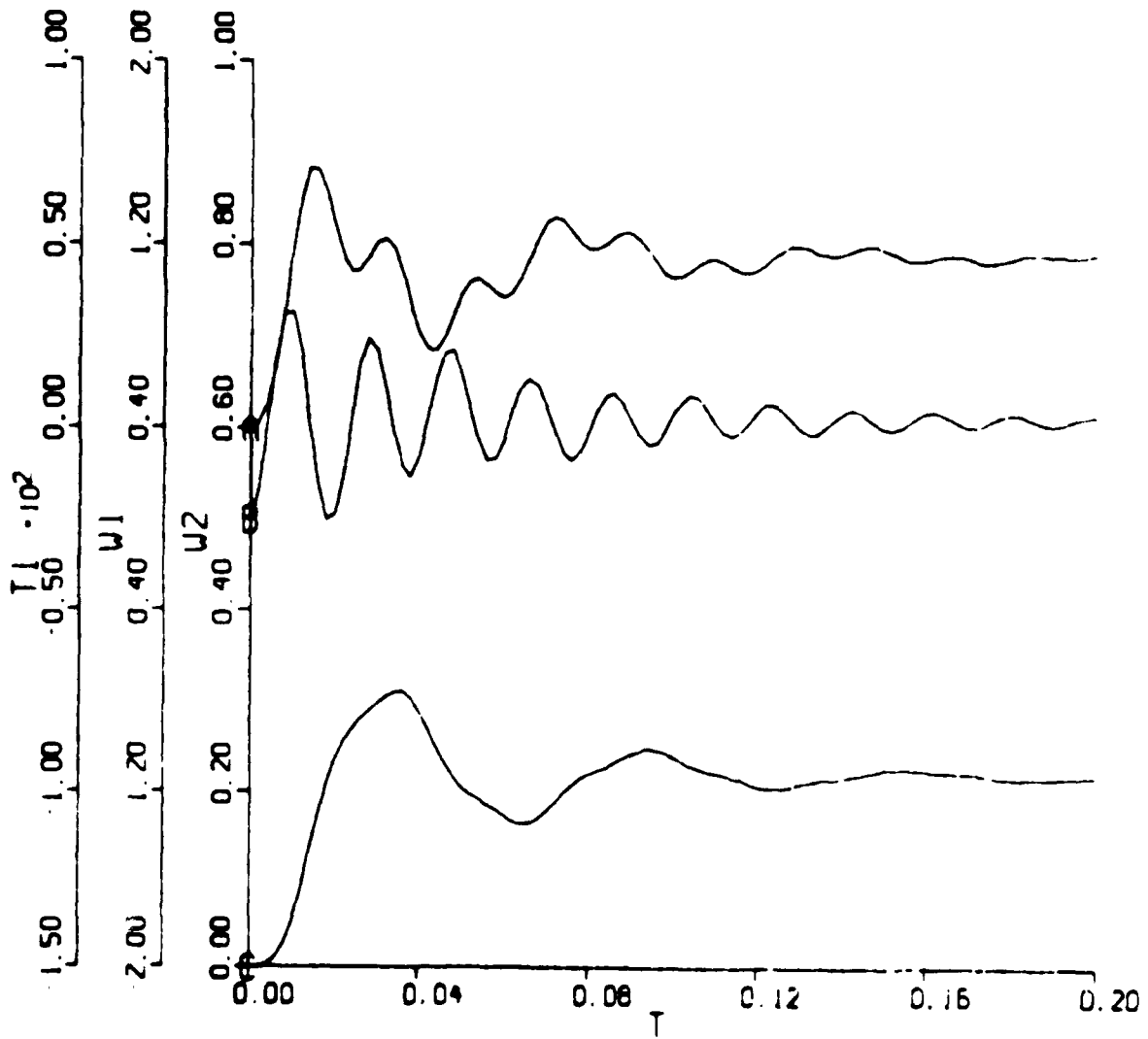


Figure 22: Pinion Torque and Motor Speed Response for Proportional Speed Control and Torque Control of Drive Motor

feedback gains to each motor.

Proportional speed control may therefore be used to increase the torsional natural frequencies of the system above 55 Hz (345 rad/sec) by increasing the gain of the shaft speed control loops. For natural frequencies of about 55 Hz (345 rad/sec), the speed control loop gains, K_1 and K_4 , were about 700 V/(rad/sec). Torque response time was improved by increasing the torque feedback to either or both motors. In general, the optimum response was achieved when the gains of each of the respective motor speed feedback terms were of similar magnitudes and the torque gain was set at .0025 of the speed gain. For the speed gains listed above, the torque gain, K_2 or K_3 , should be about 2.0 V/(ft-lbf). The gains for proportional control are summarized below.

$$K_1 = 700 \text{ V/(rad/sec)}$$

$$K_2 = 0$$

$$K_3 = 2.0 \text{ V/(ft-lbf)}$$

$$K_4 = 700 \text{ V/(rad/sec)}$$

The torque control gains may be reversed, K_2 equal to 2.0 V/(ft-lbf) and K_3 set to zero, for similar response.

The dual input/dual output transfer functions for the proportional gains listed above were computed and are shown in Figure 24. Although, the natural

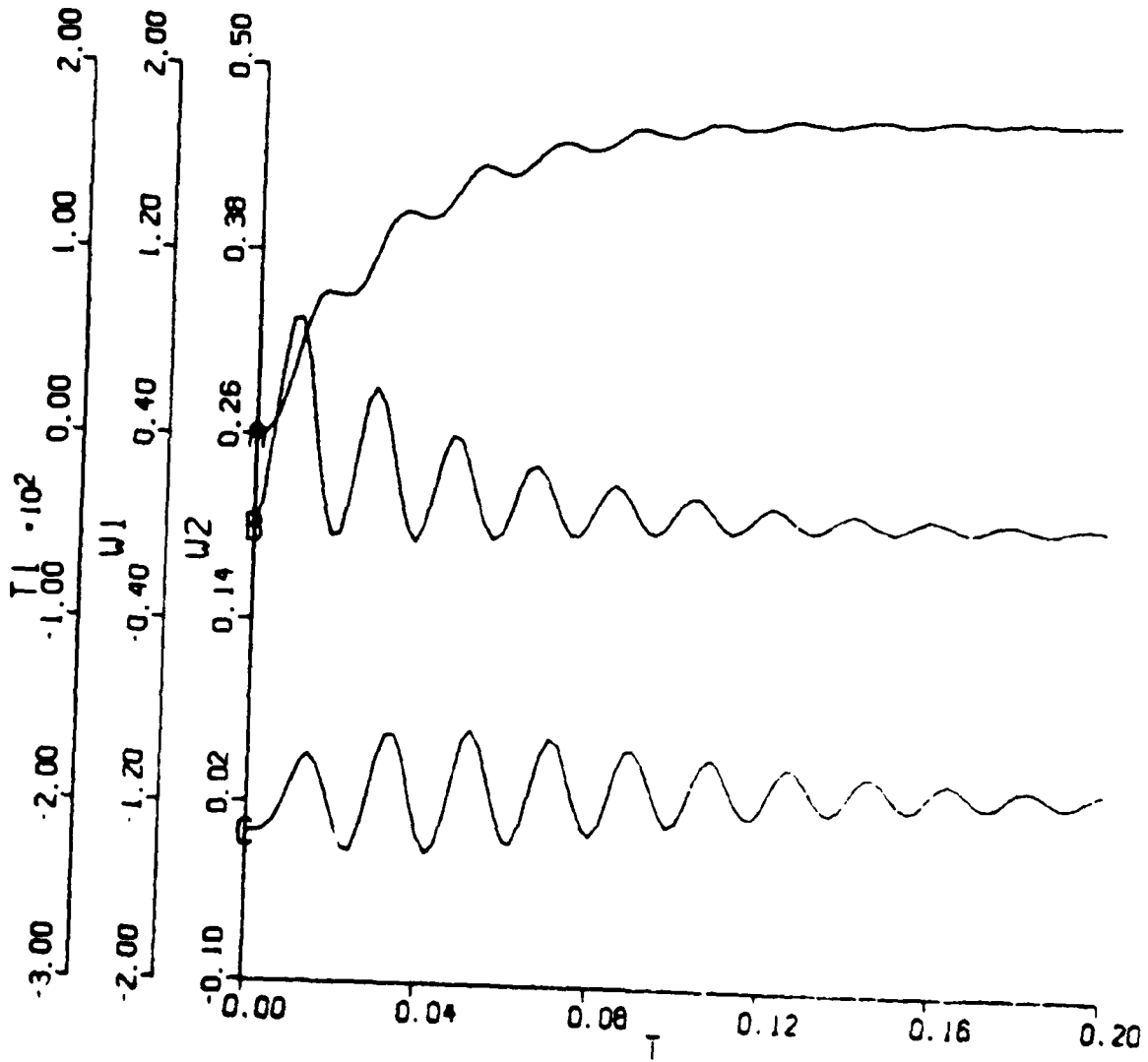


Figure 23: Engine Torque and Motor Speed Response for Proportional Speed Control of Both Motors and Proportional Torque Control of Drive Motor

frequencies are about 55 Hz (345 rad/sec), the damping ratios are observed to be too low, about 0.1 and 0.02.

4.5 Derivative Control

The block diagram of Figure 20 was modified to include derivative control as shown in Figure 25.

Proportional plus derivative (P-D) drive motor torque control, K_2 and τ_2 , was input to the drive motor. Since it was shown in the previous section that shaft speed feedback was required for stability when torque feedback was input to either motor, proportional drive motor speed control, K_1 , was added. In general, the addition of derivative torque control did not improve the response of the shaft torque, as the motor shaft speed oscillations constrained the control of the torque. Similar results were obtained with P-D load motor torque control, K_3 and τ_3 , while K_2 and τ_2 were set to zero.

P-D speed control was applied to the drive motor, K_1 and τ_1 , while all other gains K_2 , τ_2 , K_3 , τ_3 , K_4 , and τ_4 were set to zero. The derivative gain, τ_1 , enabled the manipulation of the system damping ratio of the response of the drive motor speed so that values between 0.6 and to 1.0 could be achieved. As with proportional

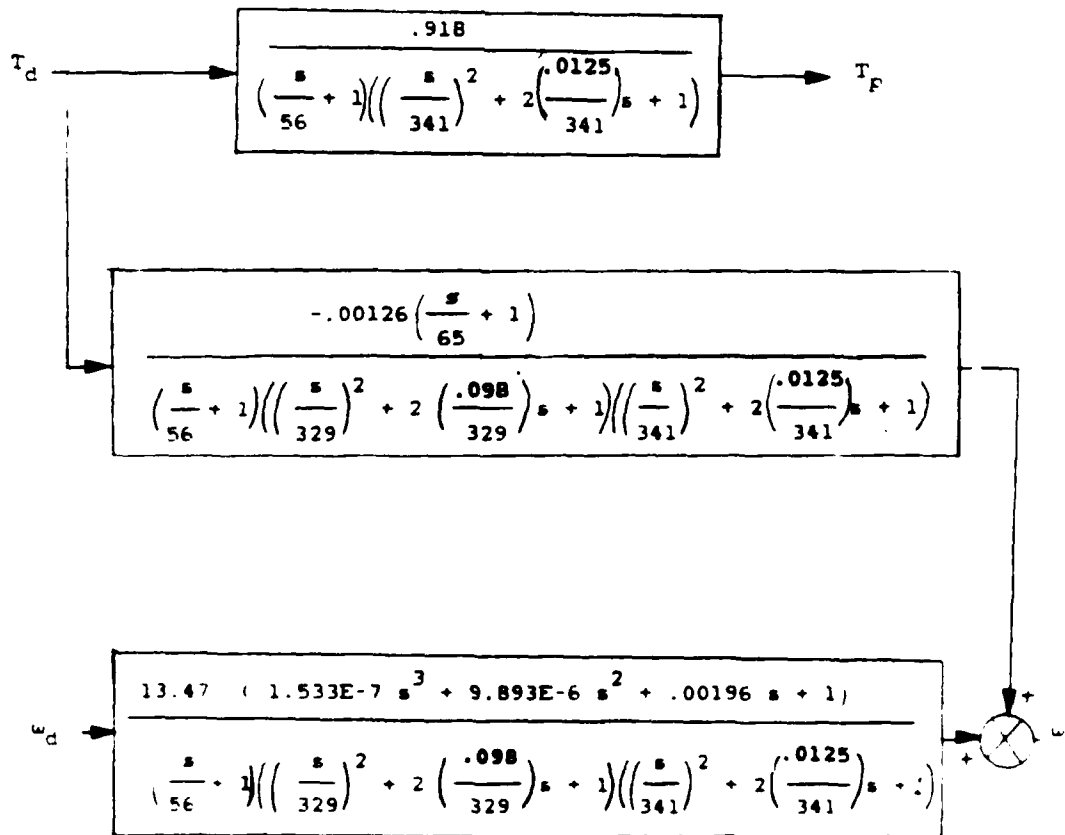


Figure 24: Closed Loop Transfer Functions with Proportional Control for the Dual Input Dual Output Block Diagram

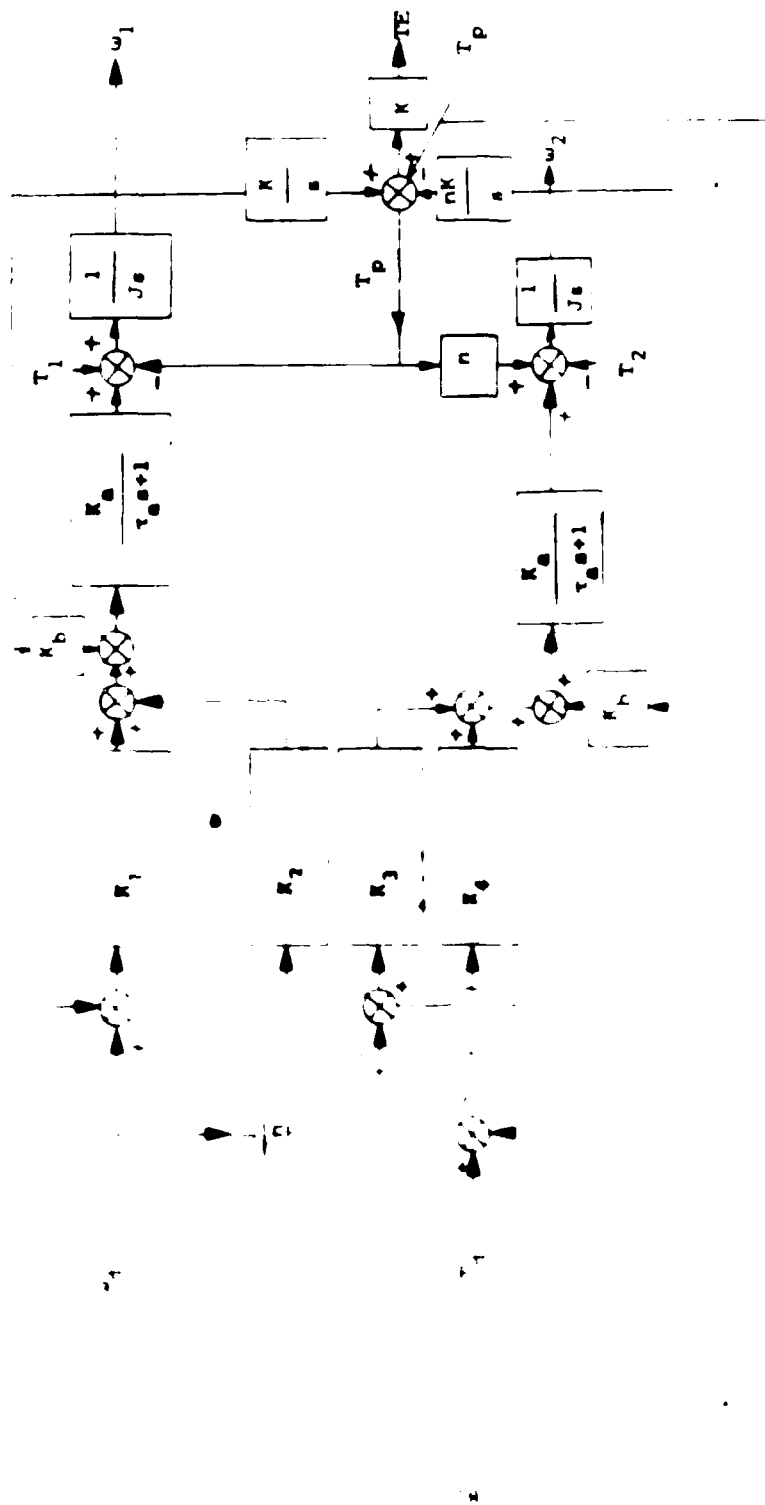


Figure 25: A two-loop control system with derivative control.

control, the responses of the drive motor speed was relatively uncoupled from the torque dynamics and the dynamics of the load motor shaft as shown in Figure 26. Again, similar results were obtained with P-D control of the load motor speed. Approximate values for a damping ratio of about 0.5 to 0.7 are achieved using a derivative gain of 0.0030 of the proportional gain. Combining the P-D speed control for each motor loop provided manipulation of the response of each motor speed.

Since the response of the pinion torque was sluggish with only P-D motor speed control, proportional drive motor torque control was added. The gain on the torque control loop, K_2 , was also somewhat uncoupled as it improved the response of the shaft torque, while the response of each motor speed remained essentially unchanged as shown in Figure 27. Similar results were obtained with proportional load motor torque control, K_3 , with either the drive motor torque gain, K_2 , set to zero or with proportional torque control from both motors, K_2 and K_3 .

Therefore, complete control of the system performance can be achieved by using p-d control of each motor speed and proportional control in the torque loop.

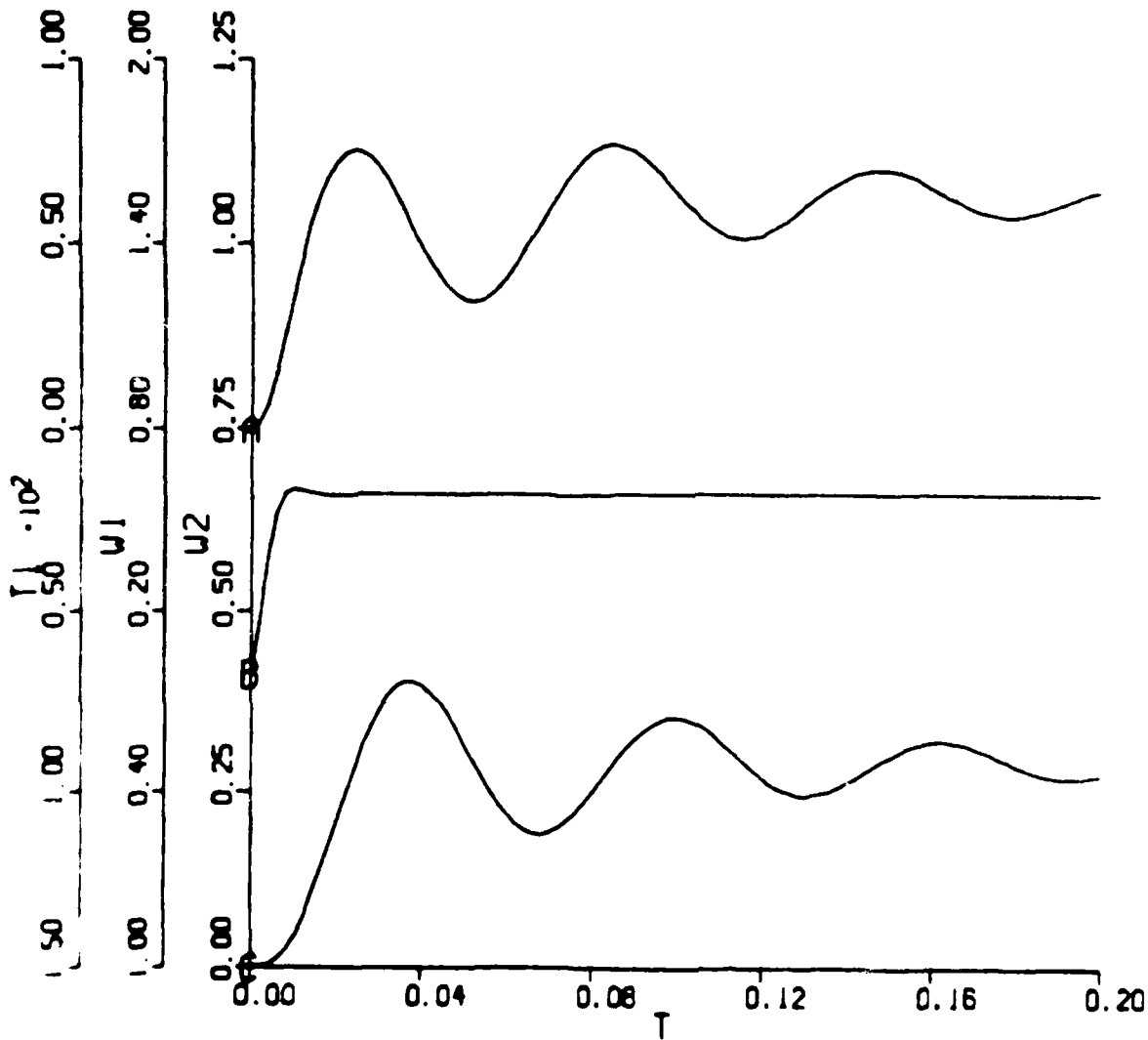


Figure 2.5. Torque and Motor Speed Response for Proportional Plus Derivative Speed Control of the Drive Motor

Torque gain was approximately 0.0060 of the proportional speed gain to each motor. The derivative control did not dominate, but did reduce the natural frequencies of the system. Hence, the proportional speed control loop gains rose to about 1,200 V/(rad/sec) for natural frequencies of about 55 Hz (345 rad/sec). The derivative speed control gains were then 3.6 V-sec/(rad/sec), while the proportional torque control gain was about 7.5 V/(ft-lbf). The proportional and derivative gains are summarized below.

$$K_1 = 1,200 \text{ V/(rad/sec)}$$

$$\tau_1 = 3.6 \text{ V-sec/(rad/sec)}$$

$$K_2 = 0$$

$$\tau_2 = 0$$

$$K_3 = 7.5 \text{ V/(ft-lbf)}$$

$$\tau_3 = 0$$

$$K_4 = 1,200 \text{ V/(rad/sec)}$$

$$\tau_4 = 3.6 \text{ V-sec/(rad/sec)}$$

The torque control gains may be reversed, K_2 equal to 7.5 V/(ft-lbf) and K_3 set to zero, for similar response.

After attaining these values, the dual input/dual output transfer functions were calculated and are shown in Figure 28. These functions were plotted from the matrix frequency program as were the disturbance input

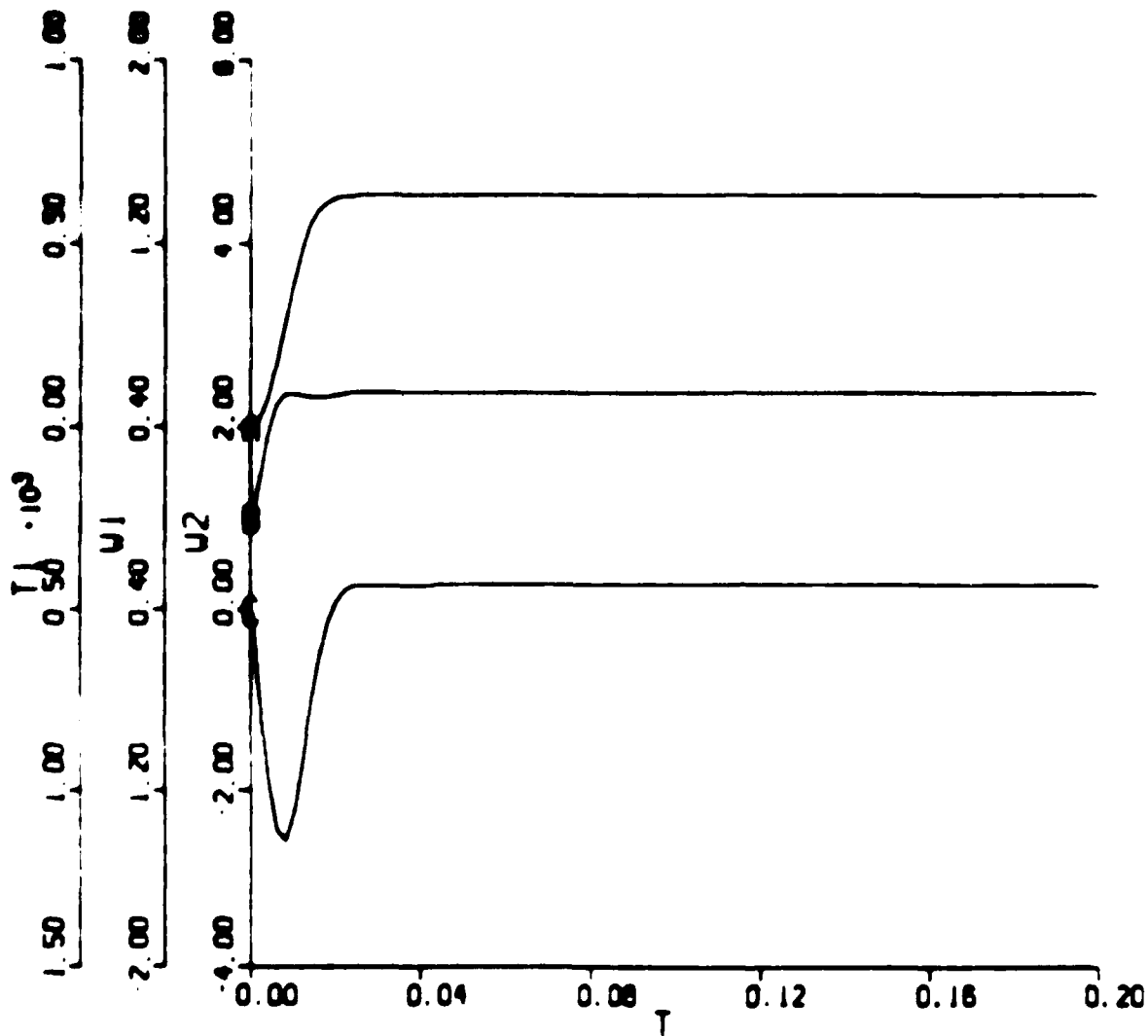


Figure 27: Finion Torque and Motor Speed Response for Proportional Plus Derivative Speed Control of Both Motors and Proportional Torque Control of the Load Motor

frequency response plots as shown in Figures 29, 30, and 31. The open loop system is shown in dashed lines for comparison purposes. Clearly, there is a major reduction in each disturbance transfer function when using the proportional and derivative control algorithms.

4.6 Integral Control

Integral control was implemented in all modes, but was found to have a negligible effect on the step responses of either motor speed or the pinion torque. Integral control may likely reduce the steady state errors, but this is of minor importance for the prime concern is maintaining a steady value.

4.7 Closed Loop Response

The following comments were arrived at from viewing the time domain plots and the roots of the characteristic equation:

1. The drive motor speed, the load motor speed, and the shaft torque control loops were generally uncoupled.
2. The system natural frequencies were increased by increasing the proportional gain on each proportional speed feedback signal. Each feedback signal determined one natural frequency. As the proportional gains increased, the damping ratios decreased.

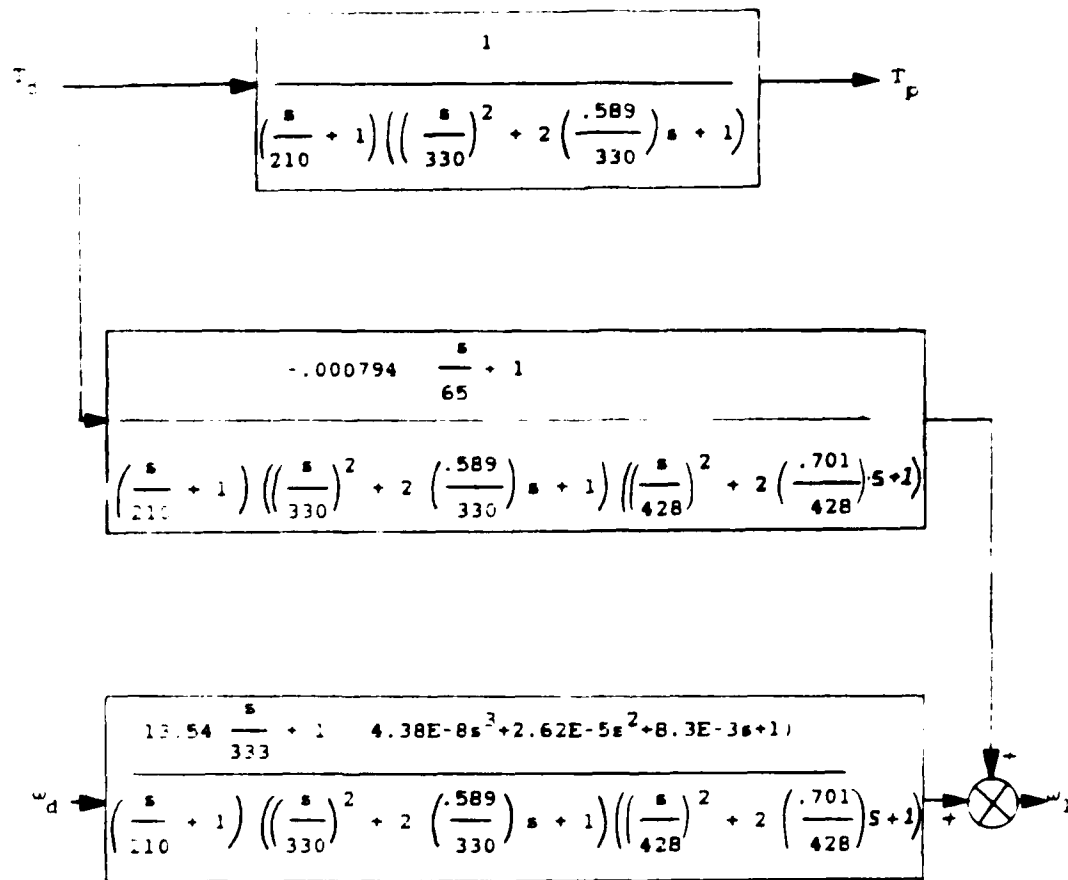


Figure 28: Closed Loop Transfer Functions with Proportional Plus Derivative Control for the Dual Input/Dual Output Block Diagram

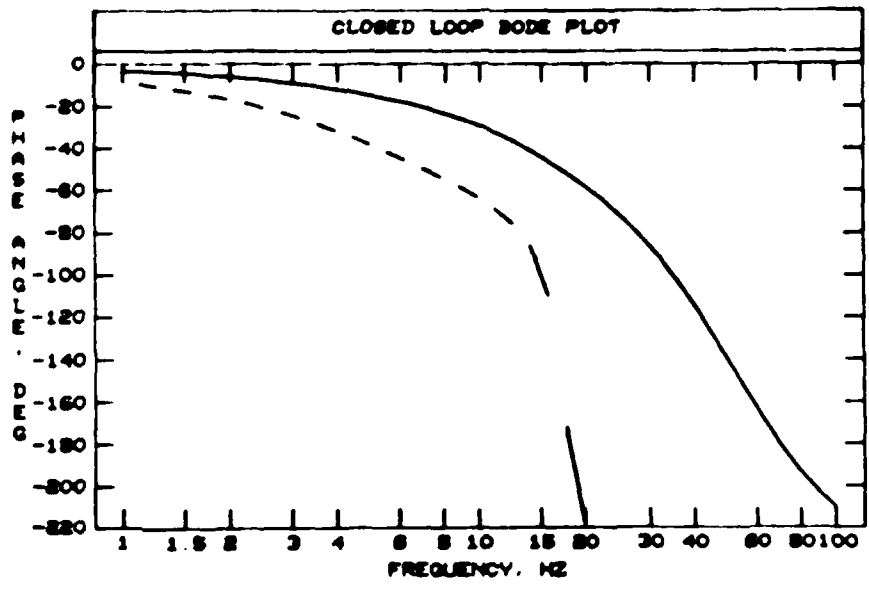
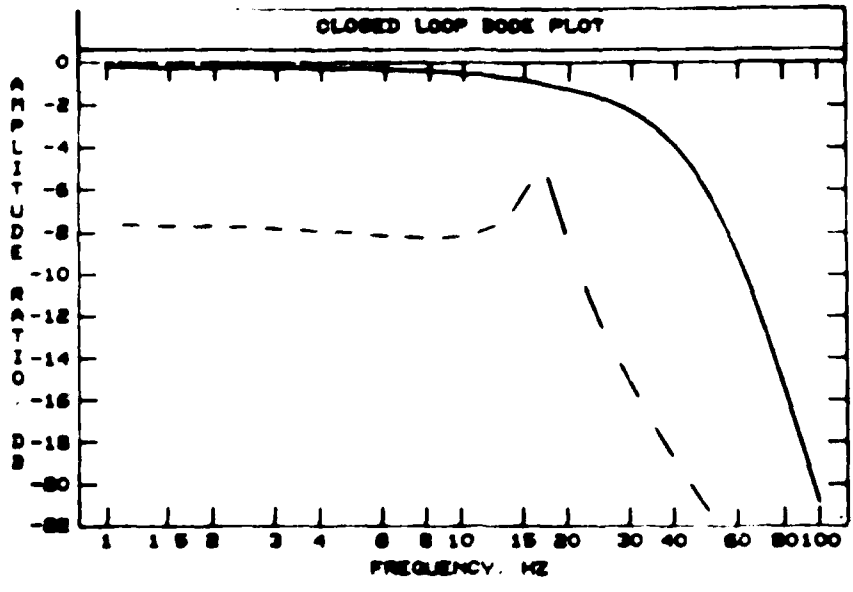


Figure 29: Bode Plot of Pinion Torque Output for a Desired Pinion Torque Input for the System with Proportional Plus Derivative Control

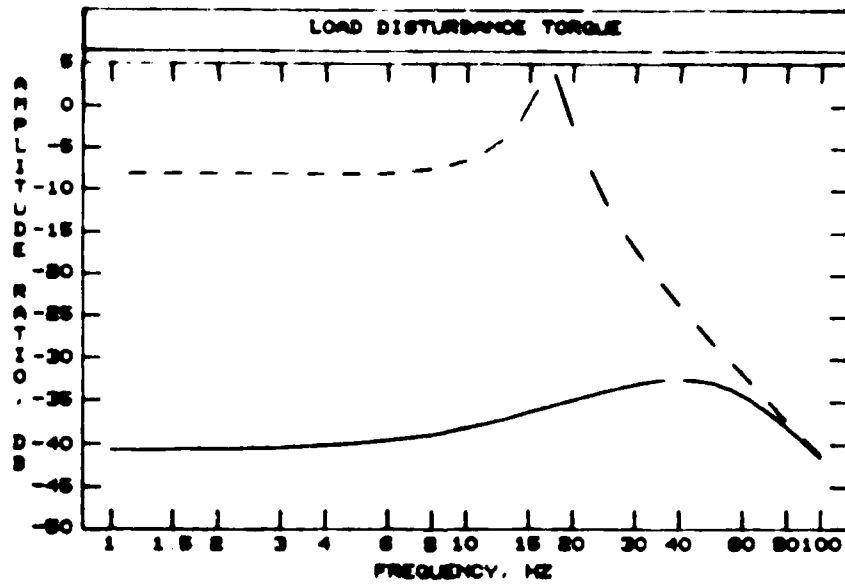
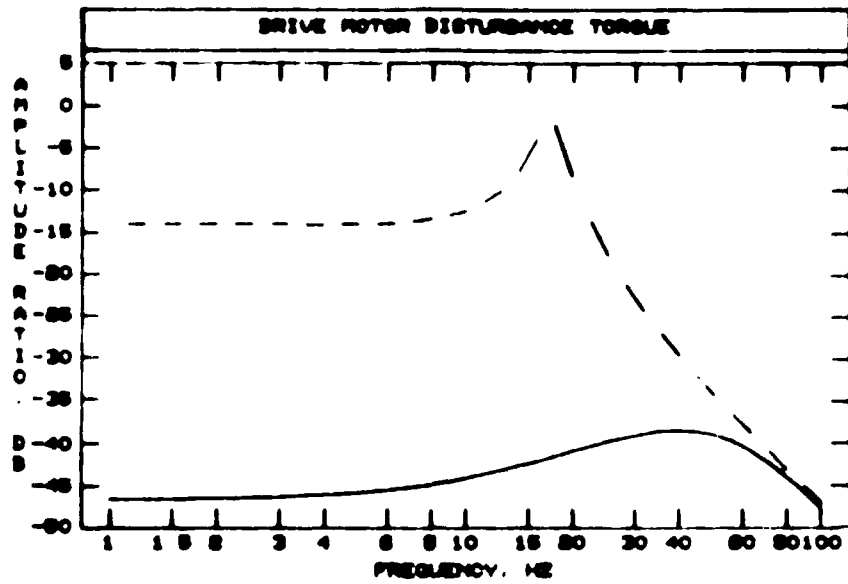


Figure 30: Bode Plot of Pinion Torque Output for a Sinusoidal Disturbance Torque Input for a System with Proportional Plus Derivative Control

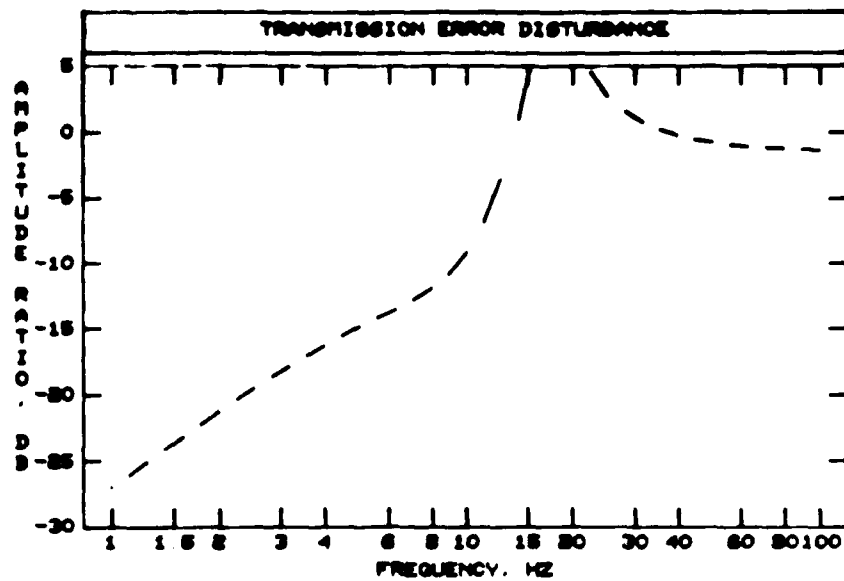
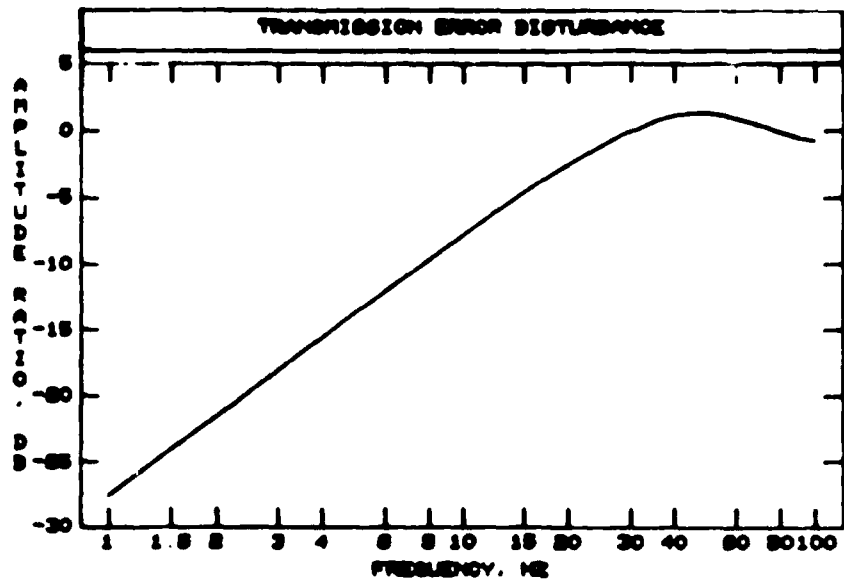


Figure 31: Bode Plot of Pinion Torque Output for a Sinusoidal Disturbance Input of Transmission Error for a System with Proportional Plus Derivative Control

3. Derivative speed control had a minor effect on the natural frequencies of the system, but increased the damping ratios and moved the one real pole closer to the imaginary axis.
4. Proportional torque control yielded an unstable system unless accompanied by speed feedback. The proportional torque gain had a small effect on the natural frequencies, but moved the real pole farther away from the imaginary axis which improved the shaft response.
5. Torque feedback of the drive motor loop was as effective as it was in the load motor loop. The gains were a function of gear ratio, i.e. for a gear ratio of two, the drive motor would require a gain which is twice the value of the load motor gain in order to produce similar results.
6. Derivative control in the torque loop was not helpful.
7. Integral control in the torque or speed feedback loops was not helpful in improving step response.
8. With speed and torque feedback in one of the motor loops (either one) the proportional gain of each loop affected the steady state value of pinion torque and shaft speed.
9. The steady state error of each motor speed and the pinion torque was reduced by increasing the proportional gain of each respective controller.

In order to achieve the design requirements stated in Section 4.1, the control regime will include proportional torque control and proportional plus derivative drive motor and load speed control. The values of gains corresponding to Figure 25 are those of

Section 4.5 and are restated below.

$$K_1 = 1,200 \text{ V}/(\text{rad}/\text{sec})$$

$$\tau_1 = 3.6 \text{ V-sec}/(\text{rad}/\text{sec})$$

$$K_2 = 0$$

$$\tau_2 = 0$$

$$K_3 = 7.5 \text{ V}/(\text{ft-lbf})$$

$$\tau_3 = 0$$

$$K_4 = 1,200 \text{ V}/(\text{rad}/\text{sec})$$

$$\tau_4 = 3.6 \text{ V-sec}/(\text{rad}/\text{sec})$$

4.8 Alternate Control Method

While implementing proportional speed control of each motor shaft speed increased the natural frequencies and essentially stiffened the system, it may be of interest to lower the torsional natural frequencies below the mesh frequency of the gear pair to make the system more compliant. Such a system would have very flexible shafts permitting the gear pair to move freely without modulating the transmitted torque.

In order to reduce the natural frequencies, negative gains would need to be implemented. Preliminary ACSL simulations indicate that the system natural frequencies can be decreased with proportional motor speed feedback, but the reduction is limited.

Increasing the proportional gain too much will make the system unstable. Neither derivative speed control nor proportional torque control have been simulated. The torque gain will likely need to be relatively small to avoid instability and might very well yield a small gain margin.

Chapter 5

ALTERNATE TEST GEAR TYPES

5.1 Introduction

Although a major portion of the gears used in industry are either spur gears or helical gears, other gear forms exist which have important and common applications. Two such types of gears are bevel gears and worm gears. With some minor modifications this test stand has the capability to test these gears.

5.2 Bevel Gears

The testing of a gear box with perpendicular shafts, i.e. bevel gears, would be possible with the addition of a thru-shaft optical encoder. Typically, the mounting fixtures of a thru-shaft encoder will be similar to a DC torque motor. The encoder will have two concentric sets of tapped holes, one for attachment to a fixed member, either the gear box, baseplate, or drive motor, and one for attachment to the shaft. Because the loading on the encoder is small and because space might

be limited, the encoder could be attached to the coupling bolts. A probable layout is shown in Figure 32.

The Gleason Goulder signal processing unit assumes that the disc density of the optical encoders are equal. In general, the output of the thru-shaft encoder will not match the 21,600 pulses per revolution of the Gleason Goulder encoders. A simple solution would be to correct for this in the number of gear teeth (of the driving gear and driven gear) inputs on the processing unit. Specifically,

$$\frac{Z_1}{Z_2} = m = \frac{Z_1}{Z_2} a = \frac{21,600}{D_d}$$

Where:

m = denotes modified gear ratio

a = denotes actual gear ratio

D_d = disc density

The conversion factor must be exact. Therefore, the thru-shaft encoder chosen should have a disc density that when divided into 21,600 is a common fraction (3/4, 4/5, 6/5, etc.).

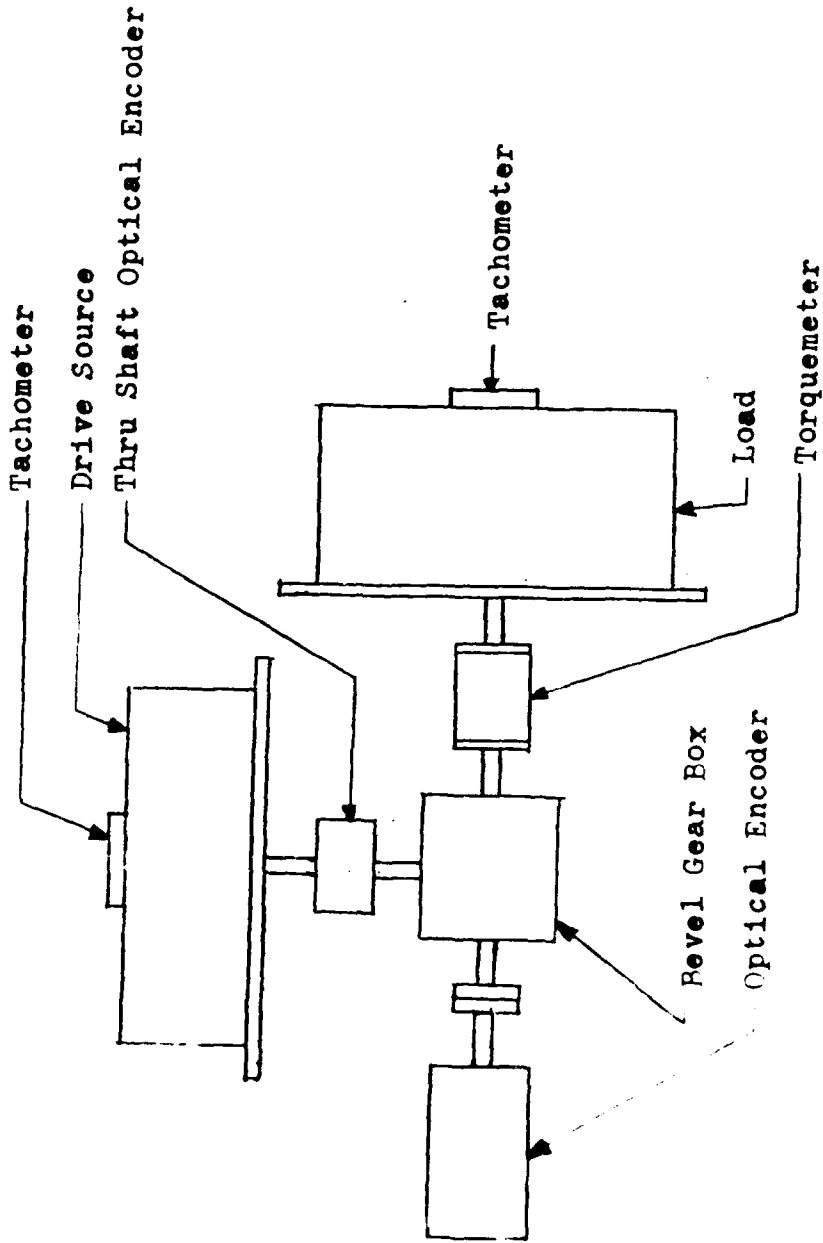


Figure 32: Revel Gear Layout

AD-A184 887

THE DESIGN AND ANALYSIS OF SINGLE FLANK TRANSMISSION
ERROR TESTER FOR LOR. (U) OHIO STATE UNIV COLUMBUS DEPT
OF MECHANICAL ENGINEERING D E BASSETT ET AL JUN 87

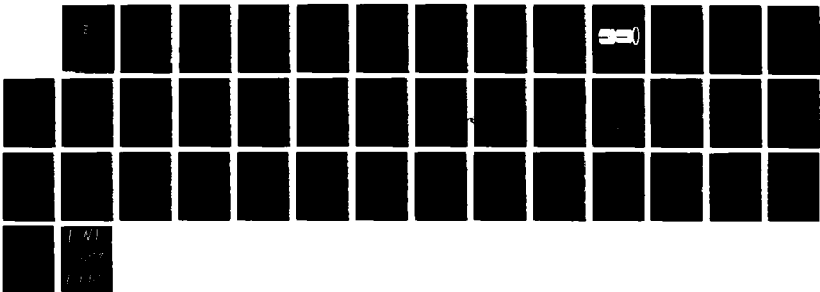
2/2

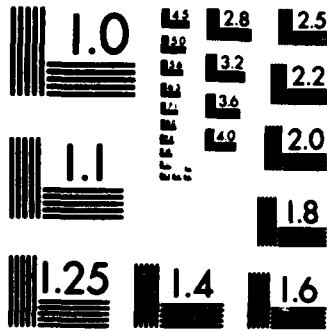
UNCLASSIFIED

NASA-CR-179621 NAG3-541

F/O 13/9

NL





MICROCOPY RESOLUTION TEST CHART
NATIONAL BUREAU OF STANDARDS-1963-A

5.3 Worm Gears

Worm gears may also be tested, but either the drive motor or load motor must be raised to accommodate the non-intersecting shaft axes. For double ended shafts on the gear box, both of the Gleason/Goulder optical encoders may be used. Otherwise, a thru-shaft encoder would again be needed for each single ended shaft. Mounting and processing unit modifications will be similar to those needed for the bevel gears. Because most worm gears have a gear ratio greater than two, the drive motor torque will be limited by the maximum load motor torque.

5.4 Alternative Transmission Error Measurement Technique

Due to the stringent speed control of the drive motor (as discussed in Chapter 4) the thru-shaft encoder needed to test a bevel gear pair or a worm gear pair might be able to be omitted. The input speed to the pinion gear would be assumed to be of constant angular velocity as Krenzer [12] did with the rear axle tester. If this can be achieved only a single encoder or torsional accelerometer would be required for transmission error measurement and the need for

thru-shaft encoders would be eliminated.

Chapter 6

Conclusions and Recommendations

6.1 Conclusions

In conclusion, the loaded transmission error test stand designed will have the capability to test a gear pair for torques up to 1400 ft*lb continuously (on the high torque side) at shaft speeds from 2-5 rpm. Measurement of the transmission error will be accomplished with high resolution optical encoders and the accompanying signal processing unit from the Gleason/Gouldner Single Flank Tester. Input power to the gear box to be tested will be supplied by a DC torque motor. Similarly, the gear box will be loaded by a DC torque motor. Electrical power to each DC torque motor will be regulated by a DC servo amplifier/controller. Proportional plus derivative speed control should be implemented for each motor, while proportional torque control can be used as a feedback loop to either the drive or load motor in order to provide for a constant torque on the gear pair.

6.2 Recommendations

1. Test Stand Operation

Although the system response was optimum with proportional plus derivative control of both motor speeds and proportional torque control to either motor, the test stand might first be run without the derivative speed (acceleration) control to either motor. The system performance may not be degraded tremendously since the command inputs of pinion torque and pinion speed are static rather than dynamic. Any oscillatory reactions would be due to drift in either command signal, ripple torque from either DC torque motor, dry friction in the bearings or gears, or transmission error. The drift of the command signal and dry friction should be minimal, while the ripple torque frequency should be sufficiently high so that its effect is minor. The transmission error was shown in Chapter 4 to have a negligible influence on the torque transmitted (by plotting the transfer function of pinion torque output for a disturbance input), but the analysis assumed a constant mesh stiffness. While this may be a good assumption for helical gears, it is a rather poor assumption for spur gears. The rapid change in stiffness of the spur gear teeth may give rise to near

step changes in torque and speed. Hence, it is advisable to use a helical gear pair for the test gears when making the system operational.

2. Base Plate Deflections

It has been suggested that baseplate and gearbox housing deflections for loaded conditions have affected the measurement of the transmission error. Measurement of these deflections and correlation to the transmission error might be beneficial. Quantitative results may be difficult, yet qualitative results might help reduce their effect on the transmission error measurement. Not much can probably be done about the rigidity of the gearbox once it has been selected, but the support of the optical encoders can be modified. Since the ground is essentially fixed the encoders could be mounted on a support that straddles the baseplate. This may very well be an awkward mounting structure, but should eliminate the movement of the encoders due to base plate deflections. The influence of the gear box deflections will still be present.

3. Optical Encoder Deflections

Gleason Works has also remarked that the deflection of the optical encoder grating due to moments from the torque loading affected the transmission error

measurement. Attaching the optical encoder after reaching operating torque offered little improvement in the test data. Ideally the flexible coupling should considerably reduce the loading effect on the encoder, but apparently significant forces are being transmitted. Since the loading may not be purely torsional, highly accurate alignment of the encoder and the gear box may not sufficiently reduce the loading effect on the transmission error measurement. Use of a more compliant coupling will suppress the loading effects, but may also suppress the true transmission error measurement.

Appendix A.

DC TORQUE MOTORS

A.1 Introduction

Since all motors produce torque, an unambiguous definition of a torque motor has never been clearly stated. However, Sierracin/Magnedyne [17], a manufacturer of DC torque motors, states that in common usage a torque motor is a motor where the emphasis in design is placed on output torque per input watt rather than output power per input watt. A consequence of this design emphasis is that most torque motors have a small length to diameter ratio, typically 1/3 to 1/10. In this configuration, which is sometimes referred to as a 'pancake', the generated electromagnetic force acts at a larger radius resulting in increased torques, but due to this geometry the mass moment of inertia of the motor also increases which, in turn, deteriorates the response times. In contrast, motors with aspect ratios above 3 have less torque capability, but have desirable response times due to their lower inertance and are useful in

servo control applications. Hence, these motors are sometimes referred to as servomotors.

Typically DC torque motors are marketed with a large inside diameter and without a frame which permits the motor to be integrated into the system design. Since DC torque motors are capable of delivering peak torque at stall (zero rpm) the motor can be directly coupled to the system without the use of an intermediate gear train. Backlash is therefore eliminated, making DC torque motors a favorable choice for positioning of slow speed-control systems. Typical applications of the large capacity torque motors include drivers for radar antennas, cat-scan machines, telescopes, and gun turrets.

A DC torque motor consists of three basic components (Figure 33): a permanent magnet (stator), an armature (rotor), and a brush assembly for commutation. The permanent magnet is usually made of one of two types of materials: Alnico and Samarium Cobalt, which generally have similar performance, but have significant differences in ease of handling. The pertinent variations of the two magnets are as follows:

1. Demagnetization of the Alnico permanent magnet will occur if the peak current applied to the motor is exceeded. The amount of

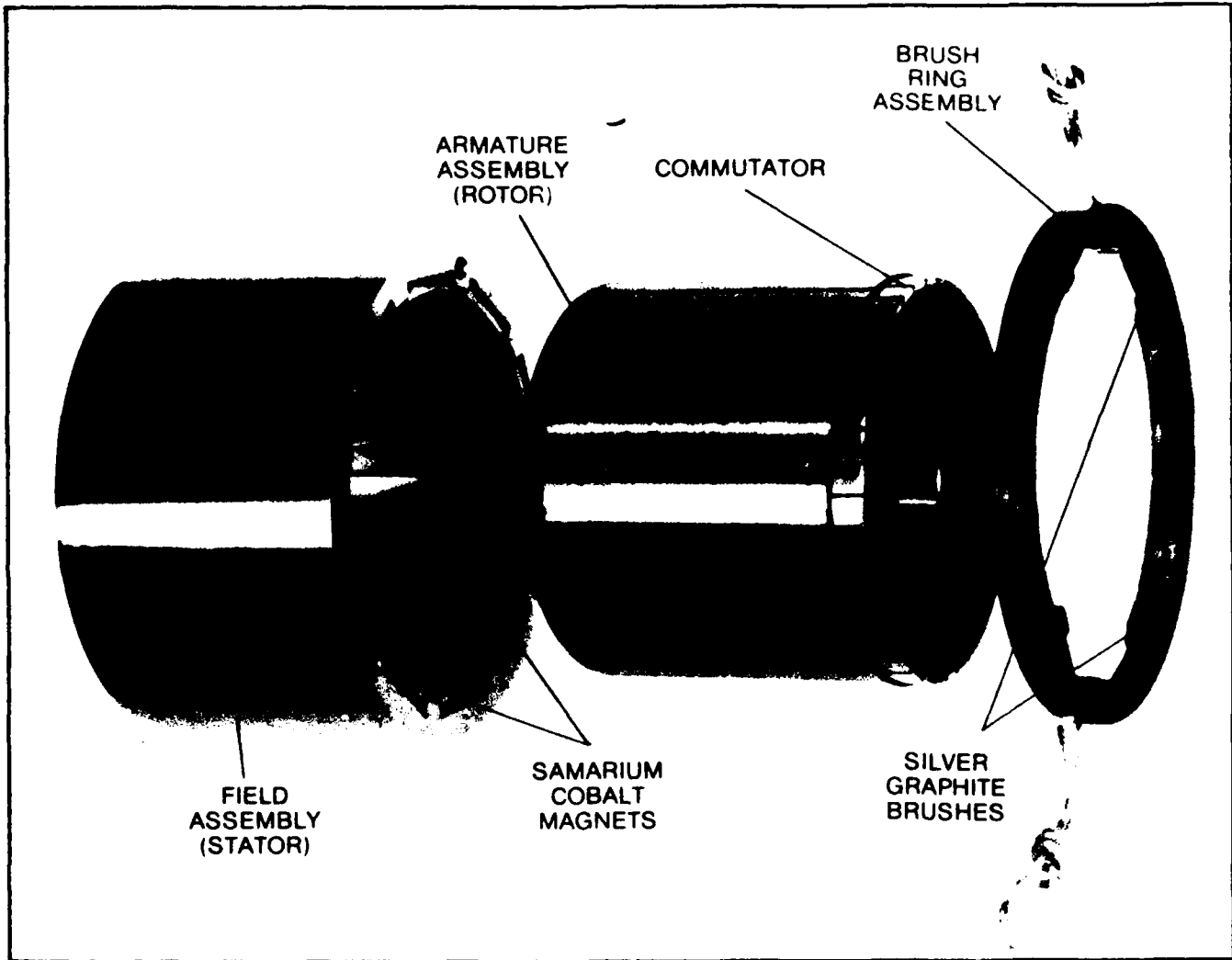


Figure 33: Basic Components of a DC Torque Motor; after [10]

demagnetization is proportional to the amount of excess current applied. Samarium Cobalt motors can handle currents above the peak current for a 'short duration' without loss to the magnet performance.

2. Samarium Cobalt motors may be designed with a thinner stator assembly resulting in less motor weight per output torque than the Alnico magnet motor.
3. Significant degradation of performance of an Alnico magnet will result if the armature is removed from the magnet because a continuous flux path must be held. Samarium Cobalt magnets can withstand an open magnetic circuit and may be separated without penalty, a feature which is quite helpful when housing the motor.
4. Alnico motors must be mounted with housings made of non-magnetic materials so that an alternate flux path from the magnet to the armature through the housing is not provided. Samarium Cobalt motors may be mounted in magnetic or non-magnetic materials.
5. Samarium Cobalt magnets are more brittle than Alnico magnets and are more likely to chip or crack, so greater care must be taken when inserting them into the housing.

Generally, the advantages of the Samarium Cobalt magnet over the Alnico magnet overshadow its disadvantages and is the preferred type of magnet for most applications.

A.2 Performance Characteristics

The electrical and mechanical elements of a DC torque motor may be modeled as shown in Figure 34. In most applications, the motor mechanical damping, B , is negligible, but electronic damping from speed feedback can improve the system stability. Kirchoff's voltage loop law may be applied to the electrical circuit to give the following:

$$0 = V_s - I (\sigma L + R) - V_b \quad (\text{A.1})$$

The back emf and the torque developed in a DC permanent magnet motor are related by the following equations:

$$T = K_t I \quad (\text{A.2})$$

$$V_b = K_b \omega$$

$$K_b = 1.356 K_t \quad (\text{A.3})$$

It can be shown that the two motor constants, K_t and K_b , are one and the same [4], but both exist because they are represented in different units (but the units are compatible). In the English system, typical units of K_b are volts/(rad/sec), while K_t 's units are ft-lbf/amp. The conversion factor is shown in equation (A.3).

The voltage/current requirements for the motor may

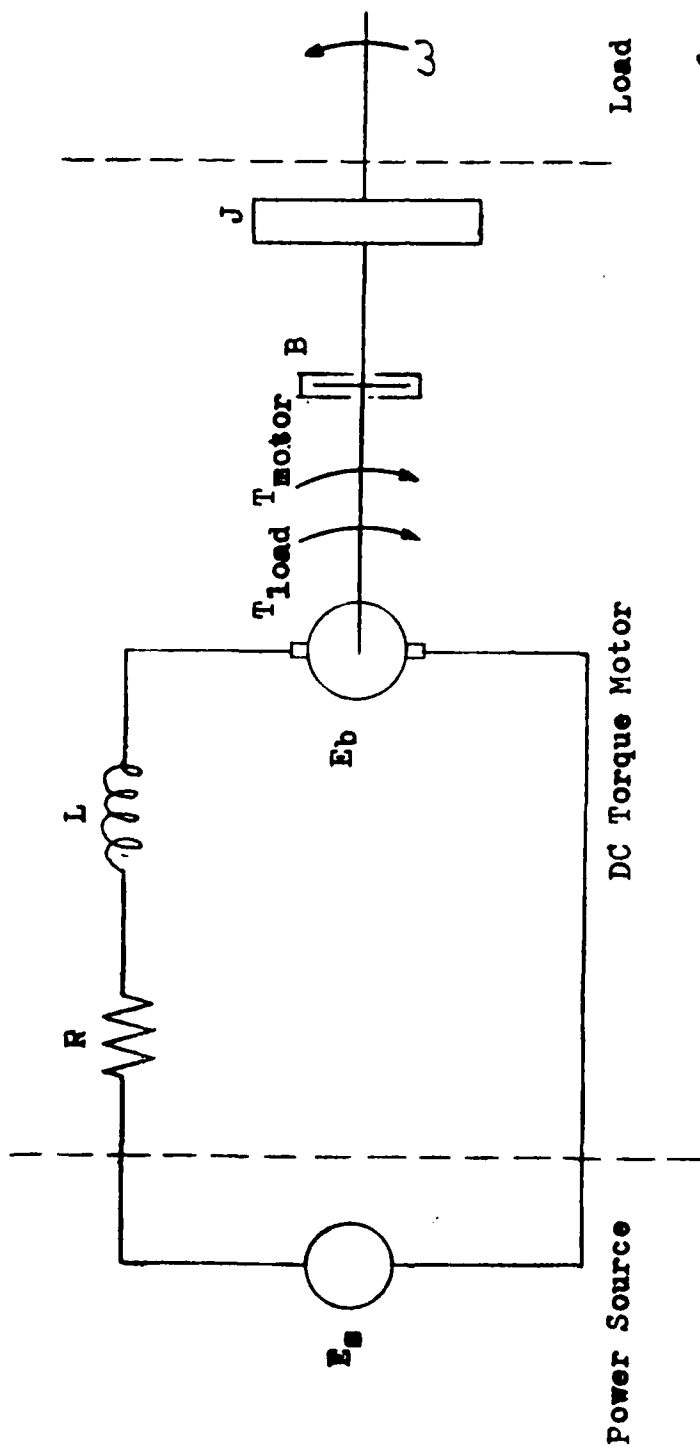


Figure 34: Model of a DC Torque Motor

be increased/decreased (or decreased/increased) to match the capabilities of the servo amplifier by changing the diameter of the armature windings. Within physical limitations (the winding cannot be too small or too thick) the performance of the motor is not affected by the choice of the winding designation.

The theoretical steady-state torque-speed curve of the torque motor is shown in Figure 35 for lines of constant source voltage. In actuality there is static friction present and there is a torque ripple due to the finite number of commutator slots on the motor. The ripple is usually less than 4% of the average torque.

A.3 Operating Limits

There are three limitations of the DC torque motor: current, voltage, and armature (or winding) temperature. Demagnetization of the permanent magnet will result if the applied current exceeds the peak current. As noted previously, this limit is more applicable to Alnico motors than Samarium Cobalt motors due to the nature of the material.

At increased voltages, arcing between the commutators and the brush assembly may occur. The parameter that indicates the amount of arcing is the

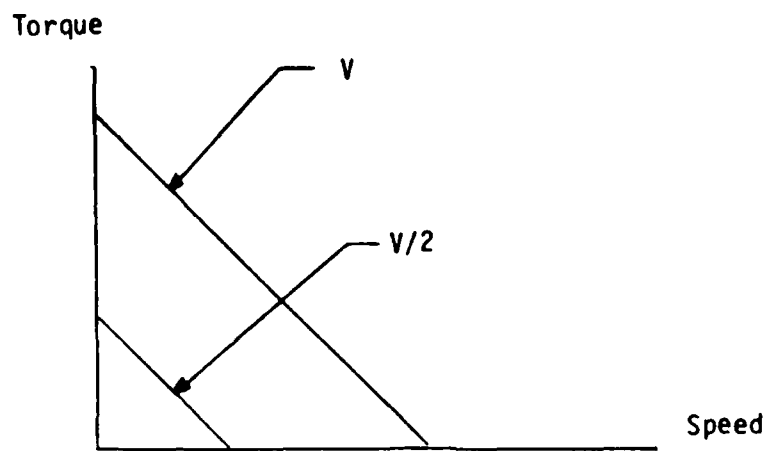


Figure 35: Theoretical Torque-Speed Curve of a DC Torque Motor

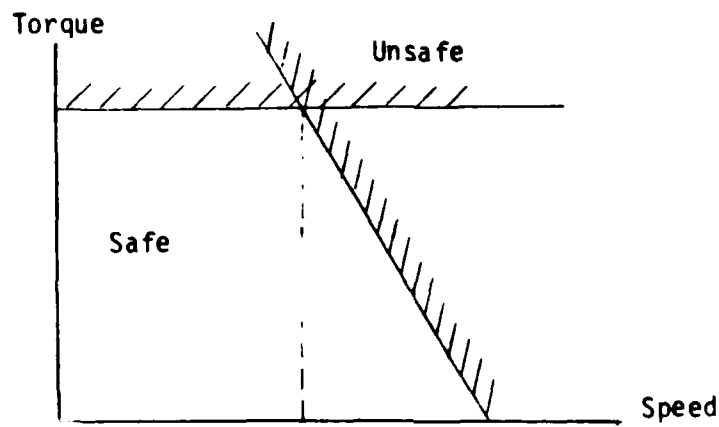


Figure 36: Torque-Speed Limitations of a DC Torque Motor

volts per bar induced, and depending on the manufacturer will generally will be around 10 - 15 volts / bar. A bar is the number of commutator slots per pole. The volts per bar is calculated in the equation below.

$$Z = \frac{V P}{C} \quad (A.4)$$

Where:

Z = the volts per bar induced

V = applied voltage to the motor, DC volts

P = the number of poles of the magnet

C = the number of commutator slots of the armature

The maximum voltage, V_m that can be applied to the motor can be calculated by solving equation (A.4) for the supply voltage, and setting Z equal to the maximum allowable volts per bar (equation (A.4)). This value will aid in the selection of a DC controller.

$$V_m = \frac{Z C}{P}$$

Using equations (A.1) and (A.2), and substituting the maximum applied voltage, the torque-speed capabilities of the motor may be defined as below.

$$T = \frac{K_t}{R} (V_m - K_b \omega)$$

Combining the maximum current and voltage constraints will produce the torque-speed curve (Figure 36) of safe

and unsafe regions. Two speeds of interest, the maximum speed at no load and the maximum speed at peak torque, are calculated below:

$$\omega_1 = \frac{V_P - I_P R}{V_m K_b}$$

$$\omega_2 = \frac{V_m K_b}{K_b}$$

Where:

ω_1 = maximum speed at peak torque

ω_2 = maximum speed at no load

The third limitation of the motor is the maximum winding temperature which is typically 260 - 310 deg. F (130 - 155 deg. C). The temperature rise of the windings is due to the power dissipated in the winding resistance, $I^2 R$. The thermal system can be modeled as a first order system and the winding temperature, including resistance rise due to increased winding temperature, can be calculated as follows:

$$T_w = T_a + TPR(I^2 R_o (1 + \alpha(T_w - T_a))(1 - \exp(-t/\tau)))$$

Where:

(A.5)

T_w = winding temperature

T_a = ambient temperature

TPR = winding temperature rise per watt

R_o = armature resistance at 77 deg. F
(20 deg. C)

α = percent resistance rise per degree of temperature increase

t = time

τ = thermal time constant of the motor

In general, the temperature rise per watt, TPR, and the thermal time constant, Tau, are conservatively rated and are about 0.05 deg. F per watt (0.10 deg. C per watt) and 90 minutes, respectfully. In the event of prolonged heating, damage to the motors can be avoided by attaching a thermostat to the armature and feeding an on/off signal to an inhibit input on the servo amplifier/controller.

Equation (A.5) is more useful if the following changes are made:

1. I , the current, is eliminated in favor of T , the torque.
2. The winding temperature is set to the maximum value.
3. The equation is solved for t , time, rather than temperature.

The resulting equation, shown below, will give the maximum test time allowable for a given torque level.

$$t = -\tau \ln \left(1 - \frac{(K_o/T^2)(T_w - T_a)}{R_o TPR(1 + \alpha(T_w - T_a))} \right) \quad (A.6)$$

By setting time equal to infinity in equation (A.6) and rearranging, the maximum continuous torque that can be

tested may be calculated as follows:

$$T_c = K_t \text{ SQRT } \frac{T_m - T_a}{R_o \text{ TPR} (1 + \alpha (T_m - T_a))}$$

Where:

T_c = continuous torque

T_m = maximum winding temperature

Typically, the maximum continuous torque will be about one-half to three-fourths of the peak torque.

Appendix B.

TRANSMISSION ERROR MEASUREMENT

B.1 Introduction

Following a description of the mechanics of a typical optical encoder, the measurement of transmission error using optical encoders is presented. The processing method discussed is that of the Gleason/Goulder Single Flank Tester, model CSF/2.

B.2 Optical Encoders

Transmission error may be accurately measured to resolutions of less than one arc second using high precision, rotary optical encoders. A basic optical encoder is shown in Figure 37.

Mounted to the shaft is a disc with N radial, evenly spaced lines. A light source is on one side of the disc, while a grating, with the same line density as the disc, and a photosensor are fixed on the other side of the disc. The light source is usually an LED (light emitting diode), while the photosensor is often a

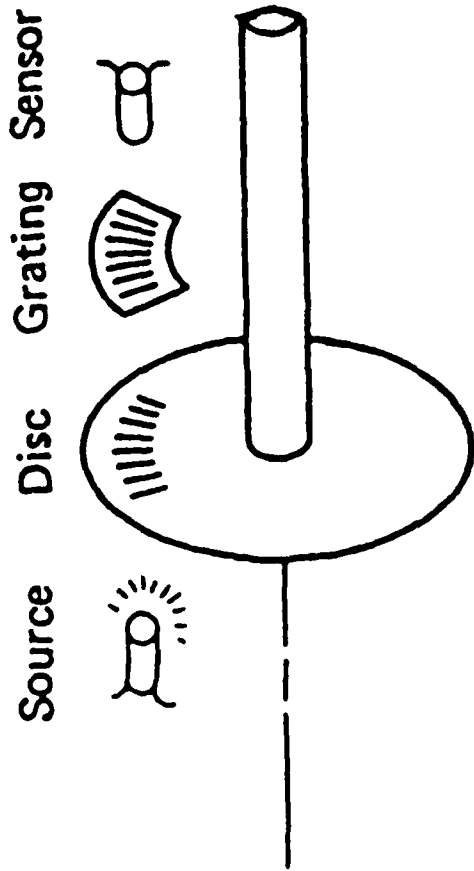


Figure 37: Basic Components of an Optical Encoder

phototransistor or a solar cell [5]. As the disc rotates, light is alternately transmitted or blocked by the disc/grating combination. The resulting output waveform of the photosensor is a quasi sine wave, which is usually amplified and squared to produce a rectangular pulse train. The frequency of this waveform, f_o , is directly proportional to disc density and shaft speed, f_s .

$$f_o = N f_s$$

Application advantages of optical encoders are their high resolution, operation down to zero speed, excellent immunity to shock and vibration, low moment of inertia, high reliability, and capability to operate over a wide range of temperatures [11]. A major disadvantage is their relatively high cost.

There are two basic types of optical encoders: absolute and incremental. They differ in that the output of the absolute encoder always represents actual shaft position, even if the power is turned off and on. The incremental encoders are significantly less expensive than the absolute encoders because there are not as many wiring components. Both types are available in solid shaft or thru shaft models. Solid shaft encoders frequently have a smaller outside diameter than

thru hole encoders and are again significantly less expensive for a given resolution.

Three common error sources in optical encoders are line spacing variations, disc concentricity, and disc flatness. Although the average frequency for each complete revolution has no error, unevenly distributed lines would generate a higher frequency in the denser regions of the disc and a lower frequency in the sparse regions of the disc. If the center of the disc line pattern is not mounted concentrically with the axis of rotation, once per revolution frequency modulation of the output occurs. A warped disc will cause amplitude modulation of the output because the illumination of the sensor depends not only on disc rotation, but disc position. The wobble modulates the blockage of the light to the sensor (Figure 3B) producing a once per revolution component. All of these errors may be substantially reduced by employing more photosensors equally spaced on the disc. Very high resolution models use as many as 8 to 12 reading stations.

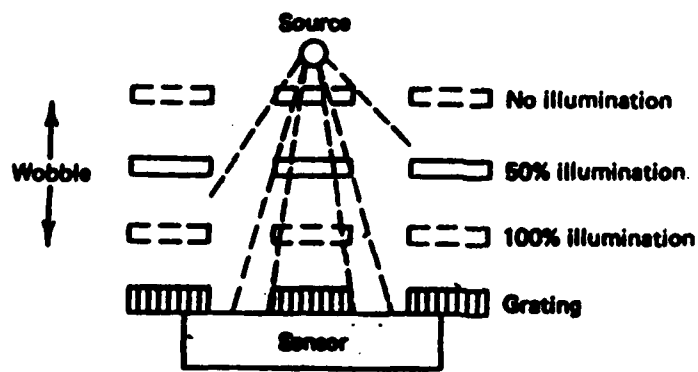
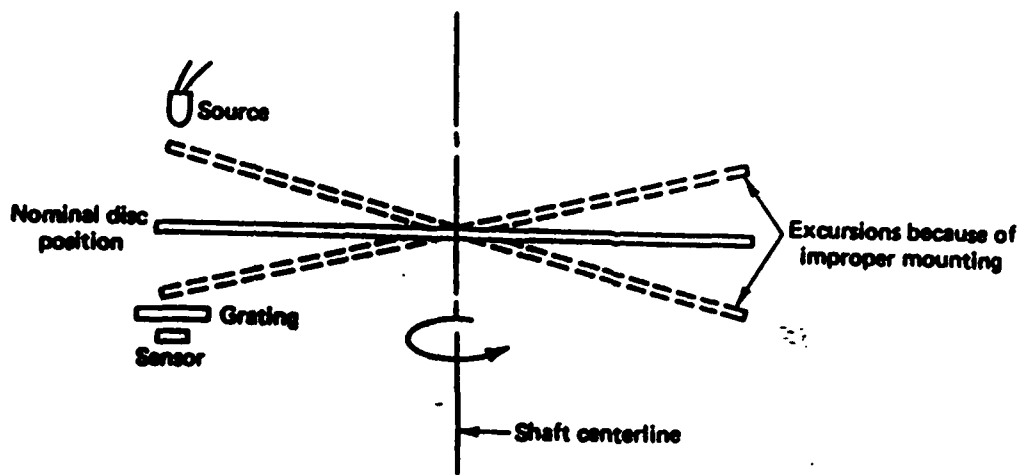


Figure 38: Effects of Disc Wobble on an Optical Encoder Sensing Unit

B.3 Signal Processing of Transmission Error

The encoder pulse train signal processing of Gleason/Goulder CSF/2 was originally designed for encoder heads made by Zeiss which had a disc density of 21,600 lines per revolution (one line per arc minute). Since then, Gleason/Goulder has used encoder heads manufactured by Heidenhain which have a disc density of 18,000 lines per revolution. Instead of modifying the existing signal processing, Gleason/Goulder multiplied the pulse train electronically inside the encoder head by 1.2 to achieve 21,600 pulses per revolution. The multiplication is accomplished by first obtaining a pulse train of 6 times the encoder output and then by using a frequency divider to divide by 5. The output waveform from each encoder is a rectangular pulse train.

To determine the transmission error from the two encoder output pulses, one signal must be frequency multiplied by the gear ratio and then the number of pulses from one waveform must be subtracted from the other as shown in Figure 39. Below is a step by step analysis of the signal processing of the Gleason/Goulder CSF/2 (Figure 40) starting with the output from the encoder heads, Figure 41a.

Following the output of the encoder heads, the

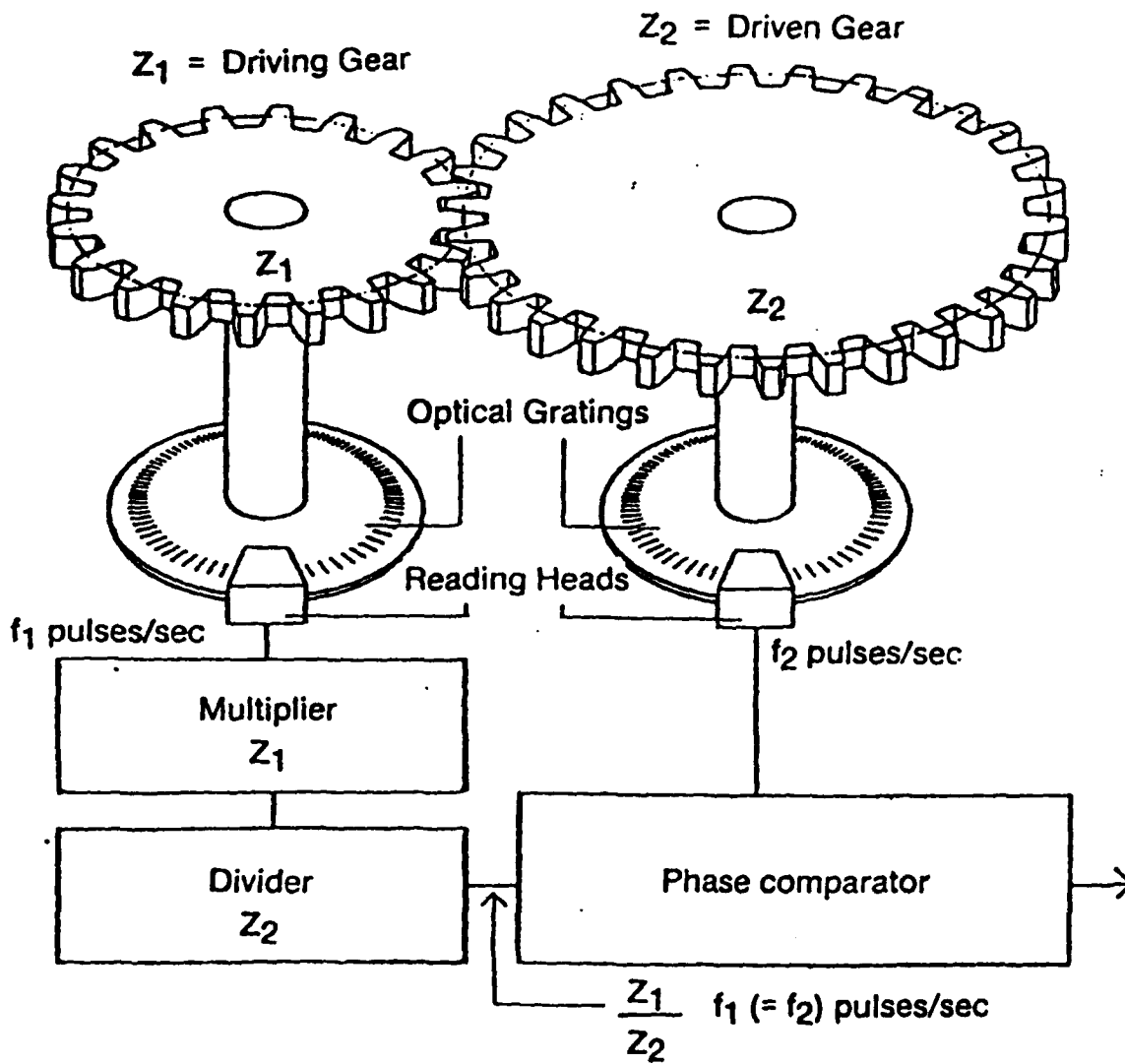


Figure 39: Calculation of Transmission Error

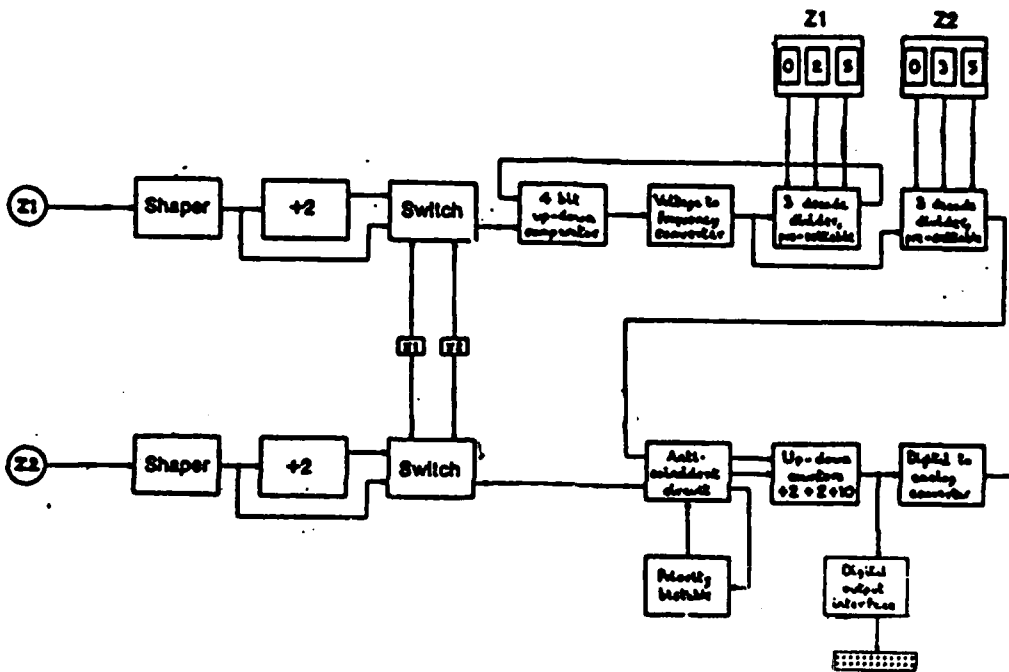


Figure 40: Gleason/Goulder Processing Electronics

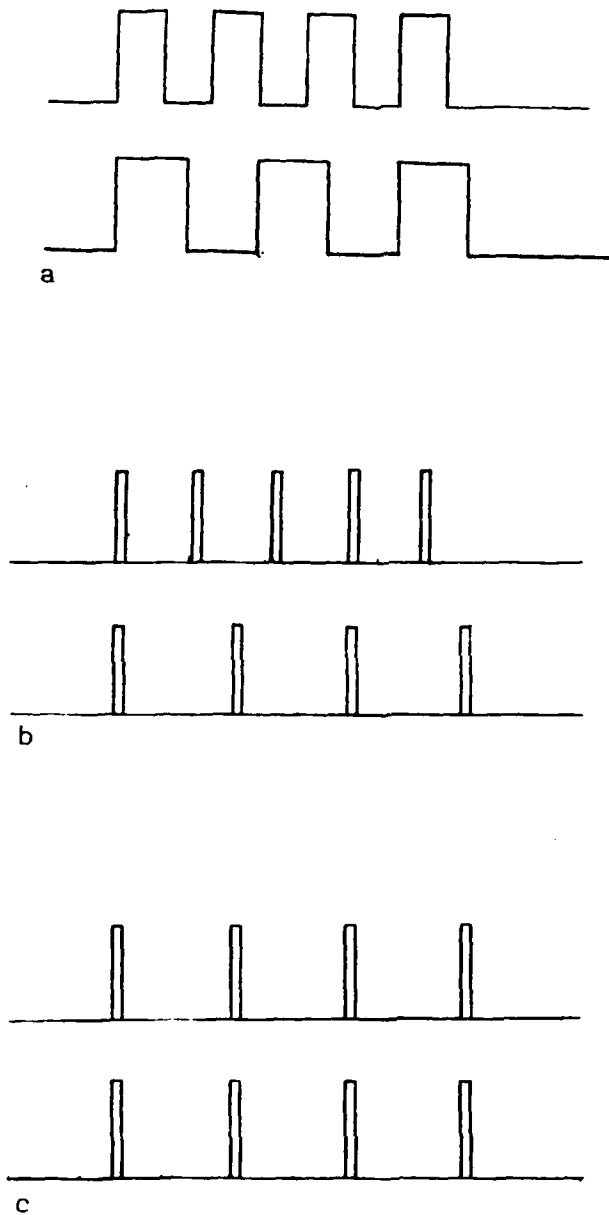


Figure 41: Frequency Multiplication of Encoder Pulse Trains

range of transmission error is selected. The standard range of 40 arc minutes may be increased to 80 arc minutes by frequency dividing each signal by 2. Frequency dividing is easily achieved by outputting 1 pulse for every 2 input pulses. Now each pulse represents an angle of 2 arc minutes, rather than of 1 arc minute.

The rectangular pulses are then passed thru a monostable which modifies the pulse to a width of 1 micro second (Figure 41b). A monostable circuit is a device that can be triggered from its normal or RESET state into a temporary SET state, from which it will trigger itself back to the RESET state after a preset time delay.

The pulse train from the driving head, f_1 , needs to be frequency multiplied by the gear ratio, Z_1 / Z_2 . The signal is first frequency multiplied by the number of teeth of the driving gear, Z_1 , and then frequency divided by the number of teeth of the driven gear, Z_2 . The multiplication is accomplished by using a frequency feedback loop, which comprises a comparator, a voltage-to-frequency converter, and a frequency divider. The comparator outputs a voltage proportional to the difference of the input frequency and the feedback

frequency. The voltage-to-frequency converter is basically an op-amp connected as an integrator which charges at a rate proportional to the output voltage of the comparator. Integrator output is compared with a fixed threshold; whenever this threshold is crossed, the integrator value is zeroed and a pulse of accurately known area is produced. The resulting pulse train of the driven head is now of the same nominal frequency as the pulse train of the driving head as shown in Figure 41c.

$$f_2 = f_1 \frac{Z_1}{Z_2}$$

The final processing of the transmission error, taking the difference of two pulse trains, is now performed. Although the driving train was frequency modified and 'traveled' thru some electronic devices, it will arrive slightly later than the signal from the driven head, but because the electronic devices operate in the nanosecond region and the pulses are at a maximum frequency of about 10 KHz, the time delay is negligible.

The two pulse trains then operate an up-down counter, which has a range of 40 discrete steps. The driving head pulses count up, while the driven head pulses count down. If a pulse from each head arrives at

the same time, the coincidence will give rise to faulty operation of the up-down counter. Therefore, an anti-coincidence circuit is included to recognize this and to inhibit both pulses whenever an unacceptable condition arises.

Since both pulses are arriving at the same nominal rate, no overall accumulation of count can occur. It is only the transient differences in repetition rate arising from the gear tooth forms which give a temporary increase or decrease in the count. If the signal were to be plotted with a digital interface, a typical waveform might look like the one shown in Figure 42. Each count or step is either 1 arc minute or 2 arc minutes depending on which range of transmission error is selected.

To obtain an analog signal of the transmission error, the discrete value is inputted into a zero order hold digital-to-analog converter. The signal may now be plotted, but since it is of 'staircase' form (with a resolution of one arc minute) it needs to be modified by low pass filtering it. The bandwidth of interest is from zero to about 10 Hz (the limit of the optical encoders); but, since the incoming pulse rate from the optical encoders is 21,600 pulses per revolution, and

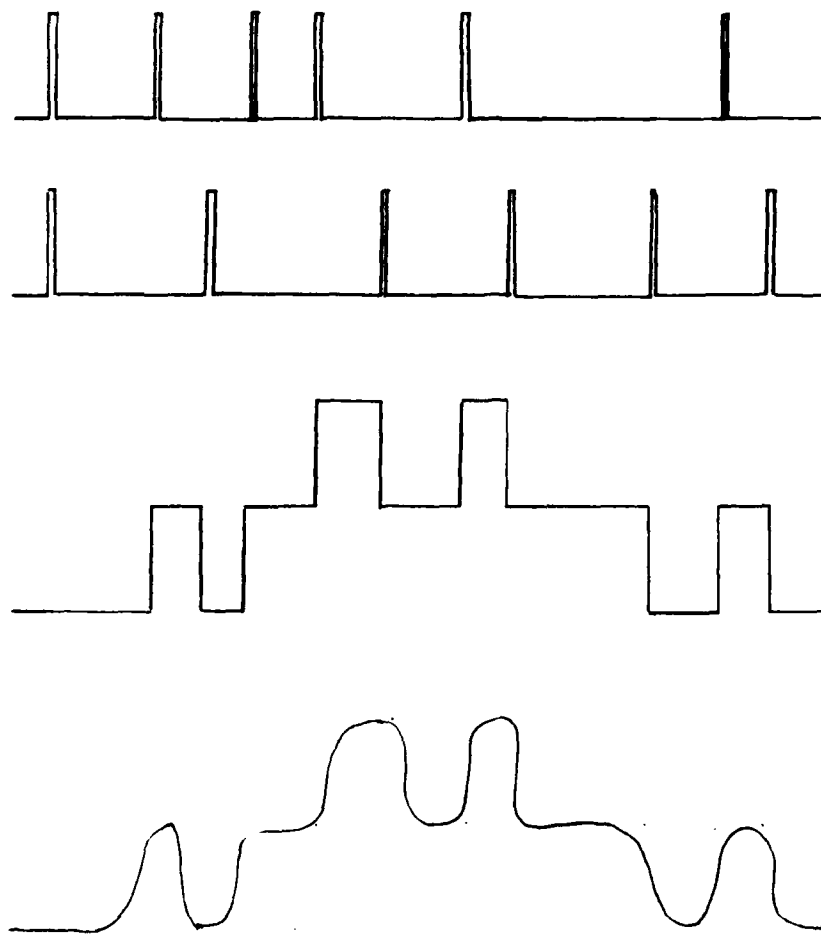


Figure 42: Digital and Analog Output of Transmission Error

maximum driving shaft speed is roughly 0.5 Hz, the transmission error signal may contain significant frequency content up to 10 KHz. After removing the high frequency content with a low pass filter, the resulting transmission error signal is now a smooth waveform. This is the transmission error of the gear train.

Error sources do exist, but a test for accuracy by using a gear pair of known tooth profiles, e.g. parabolic, the amplitudes of the frequency spectrum at tooth mesh frequency and the harmonics can be predicted and compared with measured values. Gleason/Goulder claims the resolution is on the order of 0.1 - 0.2 arc seconds, while the accuracy is in the range of 10 to 15 arc seconds [18].

Appendix C.
COMPUTER PROGRAMS

```

PROGRAM RBFD
INITIAL
CONSTANT L = .0248 , R = 1 6 , KT = 22 5 , KB = 30 6
          J = 6.1 , N = 2 , KE = 10069 , TMX = .2
          WD = 6 , TD = 600 , E10 = 0 , E20 = 0
          KDW1= 0 , KPW1= 0 , KDT1= 0 , KPT1= 0
          KDT2= 0 , KPT2= 0 , KDW2= 0 , KPW2= 0
CINTERVAL CINT = .002
END
DYNAMIC
IF ( E1 GT 100 ) E1 = 100.
IF ( E1 LT -100 ) E1 = -100.
IF ( E2 GT 100 ) E2 = 100.
IF ( E2 LT -100 ) E2 = -100.
IF ( I1 GT 100 ) I1 = 100.
IF ( I1 LT -100 ) I1 = -100.
IF ( I2 GT 100 ) I2 = 100.
IF ( I2 LT -100 ) I2 = -100.
DERIVATIVE
D1 = KDW1 * DERIVT ( 0, WD - W1 )
P1 = KPW1 * ( WD - W1 )
DT1 = KDT1 * DERIVT ( 0, - T1 )
PT1 = KPT1 * ( - T1 )
E1 = E10 + D1 + P1 + DT1 + PT1

I1 = INTEG ( ( E1 - W1 * KB - I1 * R ) / L, 0 )
W1 = INTEG ( ( I1 * KT - KE * ( TH1 - TH2 * N ) ) / J, 0 )
TH1 = INTEG ( W1, 0 )
T1 = KE * ( TH1 - TH2 * N )
TH2 = INTEG ( W2, 0 )
W2 = INTEG ( ( - I2 * KT + KE * N * ( TH1 - TH2 * N ) )
           / J, 0 )
I2 = INTEG ( ( E2 + W2 * KB - I2 * R ) / L, 0 )

E2 = E20 + D2 + P2 + DT2 + PT2
D2 = KDW2 * DERIVT ( 0, W2 )
P2 = KPW2 * ( W2 )
DT2 = KDT2 * DERIVT ( 0, TD - T1 )
PT2 = KPT2 * ( TD - T1 )
END
TERMT ( T GE. TMX )
END
END

```

```

PROGRAM RBF0
DOMAIN COMPLEX
A1 = 1200.
T1 = .003
A2 = 7.5
T2 = 0
Ka = 14.06
Ta = .0155
Kb = 30.6
n = 6.1
m = 2
A = 50345 / ( n ** 2 + 1 )
C1 = J + Ka*K1*T1
C2 = Kb + K1
C3 = n**2 + n*Ka*K2 + 1
C4 = Ta + n**2*Ta + n*Ka*K2*T2
C5 = J*Ta
A3 = C5**2
A4 = 2*C1*C5
A2 = C1**2 + 2*Ka*C2*C5 + K*C4*C5
A2 = 2*Ka*C1*C2 + K*C1*C4 + K*C3*C5
A1 = Ka**2*C2**2 + K*C1*C2 + K*Ka*C2*C4
A0 = K*Ka*C2*C3
A = ARRAY ( 6: A0, A1, A2, A3, A4, A5 )
RA = POLYROOT ( A )
R3R = REAL ( RA(3) )
R3I = IMAG ( RA(3) )
R5R = REAL ( RA(5) )
R5I = IMAG ( RA(5) )
WN3 = SQRT ( R3R ** 2 + R3I ** 2 )
WN5 = SQRT ( R5R ** 2 + R5I ** 2 )
IF ( R3R GE 0 ) R3I = 0
IF ( R5R GE 0 ) R5I = 0
C3 = COS ( ATAN ( R3I / R3R ) )
C5 = COS ( ATAN ( R5I / R5R ) )
PRINT Z3, Z5, WN3, WN5, RA, A
END
EXECUTE RBF0

```

```

EDITING TWO
1 PROGRAM
2 DOMAIN COMPLEX, ANGLES DEGREES
3 U = A1D(1.), LW = U, U1M = U, W1P = U, TPM = U, TPP = U
4 J = 6.1, TA = .0155, KA = 14.06, KB = 30.6, K = 10069, N = 2
5 K1 = 1200, T1 = .0030, K2 = 7.5, T2 = 0
6 FOR L = 1, 61, 1, LW(L) = -1+L/20., W(L) = 6.28*10**LW(L), S = W(L)*I
7 C1 = J*TA**X2 + (J+KAKK1*TI)*S + KAKKB + KAKK1
8 C2 = (N*NKX*TA + N*NKX*KAKK2*TI)*S + N*NKX + N*NKX*KAKK2
9 C3 = KAKK1*(TI*S+1), C4 = TA*S+1, C5 = N*NKX*KAKK2*(T2*S+1)
10 A = MATRIX(2,2), A(1) = C1.C4, A(2) = -C1.(C1*S+C2)/K
11 B = MATRIX(2,5), B(1) = C3.C4, B(2) = -C3.0.C1*S.NKX.C5
X12 F = VECTOR (5,0,0,0,1,0), G = INVERSE(A)*B*X
13 U1 = Q(1), U1M(L) = 20.*LOG10(ABS(U1)), W1P(L) = PHASE(U1)
14 TP = Q(2), TPM(L) = 20.*LOG10(ABS(TP)), TPP(L) = PHASE(TP)
15 IF ( W1P(L) .GT. 0 ) W1P(L) = W1P(L) - 360
16 IF ( TPP(L) .GT. 0 ) TPP(L) = TPP(L) - 360
17 ENDLOOP L
.X

```

Appendix D.

COST ANALYSIS

The funds available from the National Science Foundation and The Ohio State University for the equipment to build this test stand were \$85,510. Because of the reduced cost of the DC torque motors, some items originally not planned for will be purchased. The funds will be appropriated as follows:

	Proposal	Actuality
(1) Drive Motor	26,000	22,000
(1) Load Motor	33,800	22,000
(2) Servo Amplifiers	6,000	10,000
(2) Torquemeters and signal conditioning	9,000	9,000
(4) Eddy Current probes and signal conditioning	2,400	2,400
(2) Precision Encoder Couplings	1,200	donated
(2) Gear Couplings	360	donated
(1) Baseplate	5,800	920
Shipping and Insurance	950	1,500
(2) Tachometers	not specified	2,000
(1) Overhead Crane	not specified	1,500
(1) Slip Ring Assembly for Gear Tooth Strain Measurement	not specified	2,000
(1) Data Logger	not specified	3,000
(1) Computerized Data Acquisition	not specified	3,000
(1) Tracking Ratio Tuner	not specified	3,000
(1) Additional Strain Gage Signal Conditioning	not specified	3,000
<hr/>	<hr/>	<hr/>
Total	85,510	85,320

References

- [1] AGMA.
Gear Strength Rating 218.01 .
- [2] Daly, K.J.
Gear Drive Transmission Errors .
PhD thesis, Cambridge University, 1979.
- [3] Daly, K.J. and Smith, J.D.
Using Gratings in Driveline Noise Problems .
Proc. Noise and Vibrations of Engines and
Transmissions, I Mech E :15-20, 1979.
- [4] Electro-Craft Corp.
DC Motors, Speed Controls, Servo Systems .
Pergamon Press, Ltd., 1977.
- [5] Geiger, D.F.
Phaselock Loops for DC Motor Speed Control .
John Wiley & Sons, Inc., 1981.
- [6] Harris, S.L.
Dynamic Loads of Spur Gear Teeth .
Proc. I Mech E 172:87-112, 1958.
- [7] Hayashi, I. and Hayashi, T.
New Measuring Method of a Single Flank
Transmission Error of a Pair of Gears .
Proc. Fifth World Congress Theory of Machines and
Mechanisms, ASME :359-362, 1979.
- [8] Houser, D.R.
Research in the Gear Dynamics and Gear Noise
Research Laboratory .
SAE Technical Paper Series 821066 :15-23, 1982.
- [9] Ichimaru, K. and Hirano, F.
Dynamic Behavior of Heavy-loaded Spur Gears .
ASME Paper No. 72-PTG-14 :1-12, 1972.
- [10] Inland Motor Specialty Products Division.
Direct Drive DC Motors .
- [11] Itek Measurement Systems.
Optical Encoders .

- [12] Krenzer, T.C.
C-V Axle Tester .
1976.
Gleason Works Corp.
- [13] Litvin, F., Goldrich, R., Coy, J., and Zaretsky, E.
Kinematic Precision of Gear Trains .
Journal of Mechanisms, Transmissions, and Automation in Design 105(9):317-326, 1983.
- [14] Munro, R.G.
Effect of Geometrical Errors on the Transmission of Motion Between Gears .
Proceedings of the Institution of Mechanical Engineers 184(30):79-84, 1969/70.
- [15] Seager, D.L.
Dynamic Behavior of Helical Gears .
ASME Paper No. 69-VIBR-16 :1-5, 1969.
- [16] Sharpe, J.E. and Smith, J.D.
Pitch Information from Single Flank Tests .
Journal Mechanical Engineering Science 13(4):227-233, 1971.
- [17] Sierracin-Magnedyné.
DC Torque Motor Catalog No. T200 .
- [18] Smith, R.E.
Single Flank Gear Testing .
Gleason Works Corp.
- [19] Toda, A. and Tordion, G.V.
Approximation of Gear Transmission Error by Standard Gear Errors .
ASME Paper No. 80-C2/DET-71 :1-6, 1980.
- [20] Welbourn, D.B.
Lecture on Gear Noise .
1976.

1. Report No. NASA CR-179621 AVSCOM TR-87-C-15		2. Government Accession No.		3. Recipient's Catalog No.	
4. Title and Subtitle The Design and Analysis of Single Flank Transmission Error Tester for Loaded Gears				5. Report Date June 1987	
				6. Performing Organization Code	
7. Author(s) Duane E. Bassett and Donald R. Houser				8. Performing Organization Report No. 764038/716109	
				10. Work Unit No. 1L161102AH45 505-63-51	
9. Performing Organization Name and Address The Ohio State University Mechanical Engineering Department Columbus, Ohio 43212				11. Contract or Grant No. NAG3-541	
				13. Type of Report and Period Covered Contractor Report Final	
12. Sponsoring Agency Name and Address U.S. Army Aviation Research and Technology Activity - AVSCOM, Propulsion Directorate, Lewis Research Center, Cleveland, Ohio 44135 and NASA Lewis Research Center, Cleveland, Ohio 44135				14. Sponsoring Agency Code	
15. Supplementary Notes Project Manager, John J. Coy, Propulsion Directorate, U.S. Army Aviation Research and Technology Activity - AVSCOM, Lewis Research Center.					
16. Abstract In order to strengthen the understanding of gear transmission error and to verify mathematical models which predict transmission errors, a test stand that will mea- sure the transmission error of gear pairs under design loads has been investigated. While most transmission error testers have been used to test gear pairs under unloaded conditions, the goal of this report was to design and perform dynamic analyses of a unique tester with the capability of measuring the transmission error of gears under load. The loaded transmission error test stand will have the capa- bility to continuously load a gear pair at torques up to 16,000 in.-lb at shaft speeds from 0 to 5 rpm. Measurement of the transmission error will be accomplished with high resolution optical encoders and the accompanying signal processing unit from an existing unloaded transmission error tester. Input power to the test gear box will be supplied by a dc torque motor while the load will be applied with a similar torque motor. A dual input, dual output control system will regulate the speed and torque of the system. This control system's accuracy and dynamic response were analyzed and it was determined that proportional plus derivative speed control is needed for each motor, while an additional proportional torque control loop is needed in order to provide the precisely constant torque which is necessary in order to have error-free measurements. The components for the tester have been obtained and the test stand should be operational shortly after comple- tion of this report.					
17. Key Words (Suggested by Author(s)) Gears; Gear transmission error; Gear noise; Gear accuracy; Gear testing; Feedback control; Torque motor			18. Distribution Statement Unclassified - unlimited STAR Category 37		
19. Security Classif. (of this report) Unclassified		20. Security Classif. (of this page) Unclassified		21. No. of pages 136	22. Price* A07

END

10-87

DTIC